

Contents

1	Introduction (draft)	1
2	Related Work	5
2.1	Analytical techniques	5
2.1.1	Models	6
2.1.2	Implementations	6
2.2	Numerical techniques	8
3	Theory	9
3.1	Light and Radiometry	9
3.2	Radiometric quantities	11
3.2.1	Radiant flux	11
3.2.2	Radiant energy	11
3.2.3	Irradiance	11
3.2.4	Intensity	12
3.2.5	Radiance	13
3.2.6	Radiometric quantities for simple lights	14
3.3	Reflectance Functions	14
3.3.1	BRDF functions	15
3.3.2	Examples of BRDF functions	17
3.3.3	The rendering equation	19
3.3.4	Fresnel equations	20
3.3.5	BSSRDF functions and generalized rendering equation . .	22
3.4	Light transport and subsurface scattering	23
3.4.1	Emission	24
3.4.2	Absorption	25
3.4.3	Out-scattering	25
3.4.4	In-scattering	25

3.4.5	Final formulation of the radiative transport equation	27
3.4.6	The diffusion approximation	27
3.4.7	Standard dipole model	29
3.4.8	Directional dipole model	31
4	Method	37
4.1	Constraints and assumptions	37
4.1.1	Quality constraints	38
4.1.2	Flexibility requirements	38
4.1.3	Performance requirements	39
4.2	Method overview	39
4.2.1	Approximation of the rendering equation	44
4.3	Sampling patterns	45
4.4	Parameter acquisition	47
4.5	Environment lights	51
5	Implementation	57
5.1	Environment	57
5.2	Algorithm overview	59
5.3	Implementation details	65
5.4	Artifacts	65
5.4.1	Incorrect sampling of the G-buffer	65
5.4.2	Incorrect sampling of the cubemap	65
5.4.3	Shadow bias	66
6	Results	69
A	Model matrices	71
A.1	Model matrices	71
A.2	View Matrix	72
A.3	Projection Matrix	73
Bibliography		75

CHAPTER 1

Introduction (draft)

Subsurface scattering (SS) is a physical phenomenon that naturally occurs in a wide range of natural materials. Some of the materials that exhibit a strong SS effect in everyday life are milk, human skin and marble. Subsurface scattering is that phenomenon that occurs when light is partially absorbed by an object, bounces inside ("scatters") and finally exits the surface on another point of the material (see Figure 1.1). The phenomenon that results is generally known as *translucency*. We can see some examples of translucency in Figure 1.2

Since the beginning of computer graphics, various attempts have been performed in order to physically model subsurface scattering. Some of these models involve Monte Carlo simulations of the light entering the medium [Pharr and Hanrahan, 2000], other focus on approximating the diffusion of light within the material using an analytical approach [Jensen et al., 2001].

The first model that proposed an analytical approach was the one by Jensen et al. [2001], as an approximation of the radiative transfer equation. This approximation has then been exploited by different authors, in order to account for multi-layered materials [Donner and Jensen, 2005], heterogeneous materials [Wang et al., 2010] and thin surfaces[Wang et al., 2010]. A recent analytical approximation, proposed by Frisvad et al. [2013], extends the approximation in order to account for the directionality of the incoming light.

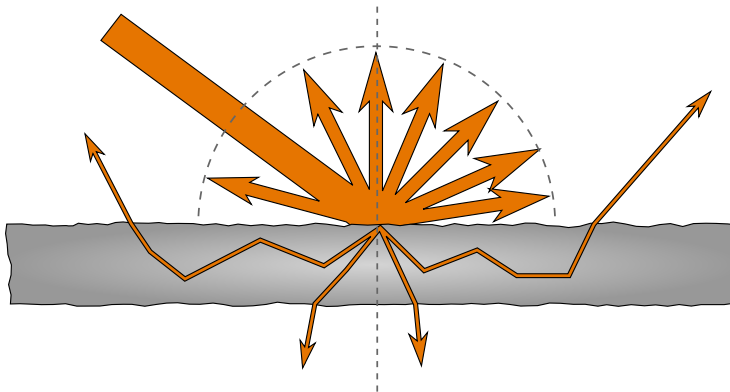


Figure 1.1: Diagram of subsurface scattering. Most of the incoming light gets reflected, but some of it enters the material and leaves it at a different point.

In recent years, with the advent of programmable graphics cards (GPU), it has become possible to exploit these algorithms and bring them to interactive frame rates, and in some cases even to real time rendering. Jensen and Buhler [2002] were the first to propose an efficient implementation (though not real time and on CPU) for rendering subsurface scattering using an octree. More recently, several methods have been proposed, including image-based splats, sum-of-Gaussians filtering, and grid-propagation based methods.

In this thesis we want to employ some cutting edge GPU techniques, with the aid of the programmable pipeline, to implement Frisvad et al. directional model in a real-time fashion. This method should achieve real time results (i.e. in the range of 30 to 60 frames per second) for a wide range of natural materials.

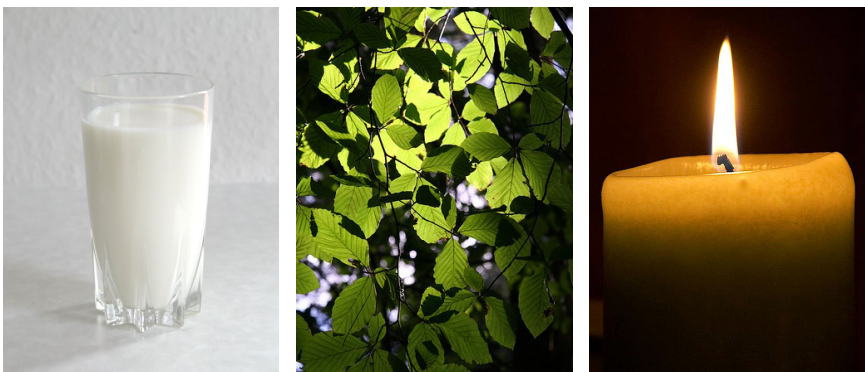


Figure 1.2: Some examples of translucent materials: milk, leaves and a candle. Images courtesy of Wikimedia Commons.

CHAPTER 2

Related Work

In rendering of subsurface scattering, all approaches rely on approximating correctly the *Radiative Transport Equation* (RTE). We identified two main approaches to the problem in literature:

Analytical One class of solutions consists of approximating the RTE or one of its approximations via an analytical model. These models can have different levels of complexity and computation times, and are often adaptable to a wide range of materials. However, often they rely on assumptions on the scattering parameters that limit their applicability.

Numerical In this other class of solutions, a numerical solution for the RTE is actually computed. While providing an exact solution, the computation times are longer. When interactivity is needed, generally some heavy pre-computation must be used.

2.1 Analytical techniques

In the analytical techniques, two different areas of research must be distinguished. The first area is the research on the actual models, while the second is

research on how the actual models can be implemented efficiently. Each model is usually represented by a specific function called BSSRDF (*Bidirectional Sub-surface Scattering Reflectance Distribution Function*), that describes how light propagates between two points on the surface. This function in the general case must be calculated between all the couple of points on the surface and then integrated over each point. Implementation techniques focus on efficiently implementing this integration step, often making assumptions for which points the computation can be avoided.

2.1.1 Models

Regarding the models, the first and most important is the dipole developed by Jensen et al. [2001]. The models relies on an approximation of the RTE called the *diffusion approximation*, that relies on the assumption on highly scattering materials. In this case, a BSSRDF for a planar surface in a semi-infinite medium can be obtained. The BSSRDF needs only the distance between two points to be calculated, and with some precautions can be also extended to arbitrary geometry. This model does not include any single scattering term, that needs to be evaluated separately. The model was then further extended in order to account for multi-layered materials[Donner and Jensen, 2005].

A significant improvement on the model was later given by D'Eon [2012], that improved the model to better fit path traced simulations without any extra computation cost. A more advanced model based on quantization was proposed by D'Eon and Irving [2011], that introduced a new physical foundation in order to improve the accuracy of the original diffusion approximation. Finally, some higher order approximation exist [Frisvad et al., 2013], in order to account for the directionality of the incoming light and single scattering. This allows a more faithful representation of the model at the price of extended computation times.

Finally, for real-time critical applications (such as games), translucency is often estimated as a function of the thickness of the material, that is used to modify a lambertian term [Tomaszewska and Stefanowski, 2012]. While not physically accurate, this technique allows to have a fast translucency effect that can be easily added to existing deferred pipelines.

2.1.2 Implementations

Most research on efficient implementations of a subsurface scattering analytical model has been made on the original model by Jensen et al. [2001]. The first

efficient implementation was proposed by Jensen and Buhler [2002], based on a two-pass hierarchical integration approach. Samples on the model are organized in an octree data structure, that then is used to render the object. In the first step, the radiance from the light is stored in the points. In the second pass, using the octree, the contribution from neighboring points is computed, clustering far points in order to speed up calculations. In the original paper, the single scattering term is approximated with as a simple BRDF approximation.

Lensch et al. [2002] approached the problem by subdividing the subsurface scattering contribution into two: a direct illumination part and a global illumination part (i.e. the light shining through the object). The global illumination part is pre-computed as vertex-to-vertex throughput and then summed to the direct illumination term in real-time. Translucent shadow maps [Dachsbaecher and Stamminger, 2003] use an approach similar to standard shadow maps: they render the scene from the light point of view, and then calculate the dipole contribution in one point only from a selected set of points, according to a specified sampling pattern. As in Lensch et al. [2002], the contribution is split into global and local to permit faster computations. Mertens et al. [2003b] propose a fast technique based on radiosity hierarchical integration techniques, that unlike the previous implementation can handle deformable geometry.

Another important category of methods is screen space methods. Mertens et al. [2003a] propose an image space GPU technique that pre-computes a set of sample points for the area integration and then performs the integral over multiple GPU passes. d'Eon et al. [2007] proposes a method in image-space, interpreting subsurface scattering as a sum of images to which a gaussian filter has been applied. The gaussians are then summed with weights that make them fit the diffusion approximation. Jimenez et al. [2009] improves further the technique, giving more precise results in case of skin. Shah et al. [2009] present a fast technique that render the object as a series of splats, using GPU blending to sum over the various contributions.

Regarding more advanced models, the better and the quantized dipole can be applied to any of the previous implementations, since they do not require additional information that the standard dipole. On the other hand, the directional dipole requires the direction of the incoming light as part of its calculations, so it is generally not applicable to the mentioned implementations.

2.2 Numerical techniques

Numerical techniques for subsurface scattering are often not specific, but come for free or as an extension of a global illumination numerical approximation, since the governing equations are essentially the same. Given their generality, they are usually slower than their analytical counterpart, and often rely on heavy pre-computation steps in order to achieve interactive framerates. Jensen’s Photon Mapping[Jensen and Christensen, 1998] was originally developed to render anisotropic subsurface scattering. Classical approaches as a full Monte-Carlo simulation implementation of the light-material interaction[Dorsey et al., 1999], and finite-difference methods exist in literature[Stam, 1995].

Some less general methods have been introduced in order to devise more efficient approximations when it comes to the specific problem of subsurface scattering. Stam [1995] uses the diffusion approximation with the finite difference method on the object discretized on a 3D grid. Fattal [2009] uses as well a 3D grid, that is swept with a structure called light propagation map, that stores the intermediate results until the simulation is complete.

Wang et al. [2010], instead of performing the simulation on a discretized 3D grid, makes the propagation directly in the mesh, converting it into a connected grid of tetrahedrons called *QuadGraph*. This grid can be optimized to be GPU cache friendly, and provide a real-time rendering of deformable heterogeneous objects. The problem in this method is that the QuadGraph is slow to compute (20 minutes for very complex meshes) and has heavy memory requirements for the GPU.

Precomputed radiance transfer methods is another class of general global illumination methods, that generally pre-compute part of the lighting and store it in tables[Donner et al., 2009], allowing to retrieve it efficiently with an additional memory cost.

A recent method called SSLPV - Subsurface Scattering Light Propagation Volumes [Børslum et al., 2011] extends a technique originally developed by Kaplanyan and Dachsbacher [2010] to propagate light efficiently in a scene using a set of discretized directions on a 3D grid. The method allows real-time execution times and deformable meshes with no added pre-computation step, with the drawback of not being physically accurate.

CHAPTER 3

Theory

In this chapter, we give a theoretical introduction to the topic dealt with in this thesis. The ultimate goal of this chapter is to introduce and describe what a analytical model for subsurface scattering is. First, we will give a brief introduction to what light is, and how we physically describe it. Secondly, we will introduce the basic radiometric quantities that will be used throughout the chapter. Then, we will describe how these quantities are related and can be used to describe light-material interaction, using reflectance functions, of which BSSRDF functions are a special case. Finally, we will introduce subsurface scattering and the diffusion approximation, concluding with a description of two BSSRDF functions actually used to describe it, by Jensen et al. [2001] and Frisvad et al. [2013].

3.1 Light and Radiometry

Light is a form of electromagnetic radiation, that propagates through space as a sinusoidal wave. Usually by *light* we usually refer to *visible light*, the small part of the electromagnetic spectrum the human eye is sensible to (see Figure 3.1). This small window is between the 380 nm of infrared and 750 nm of ultraviolet light, but the precise boundaries vary according to the environment and the

observer. Instead explicitly noted, we will use the terms light and visible light interchangeably in this report.

The study of light is usually referred as *optics*. In computer aided image synthesis, we are interested in representing faithfully how visible light propagates through a scene and how interacts with the objects and the materials in it. In addition, we are interested in lighting effects that are noticeable at human scales (1 mm - 1 km), like subsurface scattering, absorption and emission phenomena. Optics studies more effects, like diffraction, interference and quantum effects, but we are not interested in representing them because for visible light they happen on a microscopic scale (1 nm - 1 μm).

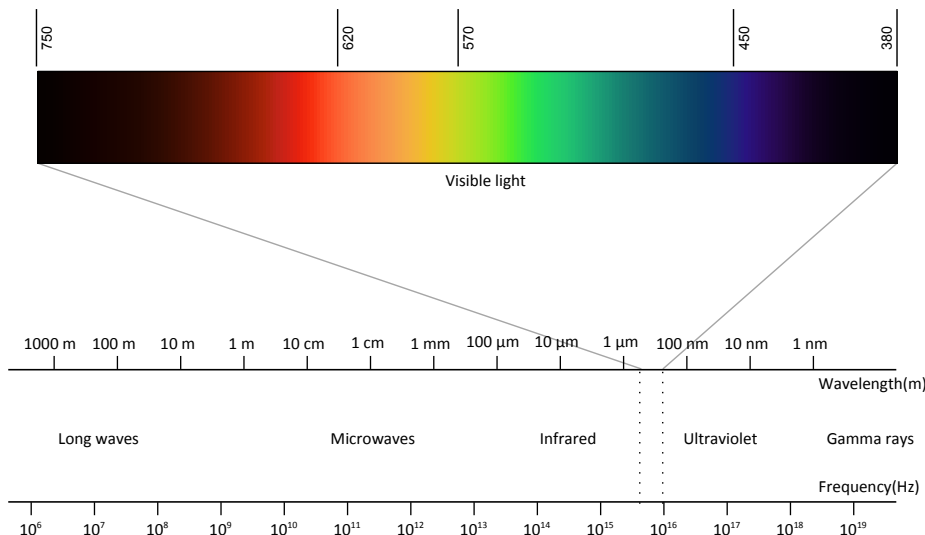


Figure 3.1: The electromagnetic spectrum.

The branch of physics that studies how to measure electromagnetic radiation is called *radiometry*. The energy of light, like all the others forms of energy, is measured in *Joules* [$\text{J} = \text{kg m s}^{-2}$], and its power in *Watts* [$\text{W} = \text{kg m s}^{-3}$]. *Photometry*, on the other hand, measures electromagnetic radiation as it is perceived from the human eye, and limits itself only to the visible spectrum, while radiometry spans all of it. The corresponding names for energy and power in photometry are *radiant energy*, measured in *talbots* [cd s], and *radiant flux*, measured in *candelas* [cd].

In image synthesis radiometry is more common, as its quantities directly derive from the electromagnetic theories, are universal, and can be easily converted to the photometric ones when necessary. The most important radiometric quantities used in computer graphics are *radiant flux*, *radiant energy*, *radiance*, *irra-*

diance and intensity.

3.2 Radiometric quantities

3.2.1 Radiant flux

The radiant flux, also known as radiant power, is the most basic quantity in radiometry. It is usually indicated with the letter Φ and it is measured in joules per seconds [J s^{-1}] or Watts [W]. The quantity indicates how much power the light irradiates per unit time.

3.2.2 Radiant energy

Radiant energy, usually indicated as Q , is the energy that the light carries in a certain amount of time. Like all the other SI units for energy, it is measured in joules [J]. Radiant energy is obtained integrating the radiant flux along time for an interval ΔT :

$$Q = \int_{\Delta T} \Phi \, dt$$

Due to the dual nature of the light, the energy carried by the light can be derived both considering the flux of photons as particles, or considering light as a wave. We will not dig further into the topic, because for rendering purposes is not important if we characterize light as a flux of particles or as a sinusoidal wave.

3.2.3 Irradiance

Irradiance, usually defined as E , is the radiometric unit that measures the radiant flux per unit area *falling* on a surface. It is measured in Watts per square meter [W m^{-2}]. It is defined as the flux per unit area:

$$E = \frac{d\Phi}{dA}$$

Irradiance is usually the term in literature used for the *incoming* power per unit area. The converse, i.e. the irradiance leaving a surface, it is usually referred as *radiant exitance* or *radiosity*, and indicated with the letter B .

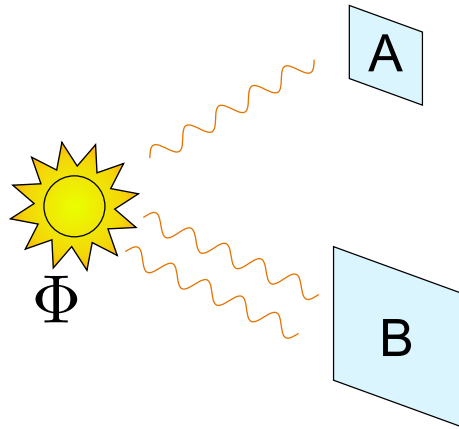


Figure 3.2: Irradiance versus power. For the two surfaces A and B , the received power Φ is the same, while the two irradiances E_A and E_B are different, as the area of B is twice as the one of A .

3.2.4 Intensity

Intensity is defined as the differential radiant flux per differential solid angle:

$$I(\vec{\omega}) = \frac{d\Phi}{d\omega}$$

It is measured in Watts per steradian [W sr^{-1}] and it is indicated with the letter I . Intensity is often a misused term in the physics community, as it is used for many different measures. Depending on the community, intensity may refer to irradiance or even to radiance (see the following section). The definition given in 3.2.4 we use the most common ddefinition given by the physics community

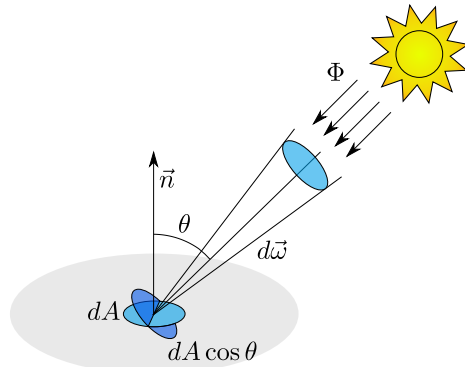


Figure 3.3: Radiance. The element of area dA gets projected according to the angle $\theta = \cos^{-1} \vec{n} \cdot \vec{\omega}$. Then the incoming flux Φ gets divided by the projected area and by the solid angle subtended by it.

3.2.5 Radiance

Radiance is arguably the most important quantity in image synthesis. It is defined precisely as the differential of the flux per solid angle per projected surface area, and it is measured in Watt per steradian per square meter [$\text{W sr}^{-1} \text{ m}^2$].

$$L(\vec{\omega}) = \frac{d^2\Phi}{d\omega dA \cos \theta}$$

Where θ is the angle between the surface normal and the incoming ray of light (so that $\cos \theta = \vec{n} \cdot \vec{\omega}_i$). Radiance has the important property of being constant along a ray of light. In addition, the sensibility of the human eye to light is directly proportional to the radiance. For a discussion on why radiance is related to the sensitivity of sensors and the human eye, see Cohen et al. [1993].

All the other radiometric quantities can be derived from radiance:

$$\begin{aligned} E &= \int_{2\pi} L_i(\vec{\omega}) \cos \theta d\omega \\ B &= \int_{2\pi} L_o(\vec{\omega}) \cos \theta d\omega \\ I(\vec{\omega}) &= \int_A L(\vec{\omega}) \cos \theta dA \\ \Phi &= \int_A \int_{2\pi} L(\vec{\omega}) \cos \theta d\omega dA \end{aligned} \tag{3.1}$$

For simplicity of notation, the dependence from the point of incidence \mathbf{x} has been dropped in equations 3.1.

3.2.6 Radiometric quantities for simple lights

To help with the formulas used later in the report, we derive the standard radiometric quantities for the two simplest types of light, i.e. directional and point lights.

- *Directional lights* simulate very distant light sources, in which all the rays of light are parallel (e.g. the sun). They are represented by a direction $\vec{\omega}_l$ and a constant radiance value, L .
- *Point lights* simulate lights closer to the observer. Isotropic point lights are represented by a position of the light \mathbf{x}_l and a constant intensity I . Point lights have a falloff that depends on the inverse square law, i.e. the radiance diminishes with the square of the distance.

Table 3.1 shows different radiometric quantities evaluated for point and directional lights, for a surface point \mathbf{x} with surface normal \vec{n} .

3.3 Reflectance Functions

After introducing the basic radiometric quantities, we still lack a rigorous way to describe light material interaction. More precisely, we need a way to relate the incoming and the outgoing radiance on a point of a chosen surface.

Quantity	Directional light	Point light
Cosine term	$\cos \theta = \vec{n} \cdot \vec{\omega}_l$	$\cos \theta = \frac{(\mathbf{x} - \mathbf{x}_l) \cdot \vec{n}}{ \mathbf{x} - \mathbf{x}_l }$
$\Phi(\mathbf{x})$ Flux	$L \delta(\vec{\omega})$	$4\pi I$
$E(\mathbf{x})$ Irradiance	$L \cos \theta$	$I \frac{\cos \theta}{ \mathbf{x}_l - \mathbf{x} ^2}$
$I(\mathbf{x}, \vec{\omega})$ Intensity	$L \delta(\vec{\omega})$	I
$L(\mathbf{x}, \vec{\omega})$ Radiance	$L \delta(\vec{\omega})$	$\frac{I}{ \mathbf{x}_l - \mathbf{x} ^2}$

Table 3.1: Different radiometric values for simple light sources.

3.3.1 BRDF functions

One of the possible way to describe light-material interaction is by using a BDRF function, acronym for *Bidirectional Reflectance Distribution Function*. The BRDF function $f(\mathbf{x}, \vec{\omega}_i, \vec{\omega}_o)$ is defined on one point \mathbf{x} of the surface as the differential ratio between the exiting radiance and the incoming irradiance:

$$f(\mathbf{x}, \vec{\omega}_i, \vec{\omega}_o) = \frac{dL_o(\mathbf{x}, \vec{\omega}_o)}{dE_i(\mathbf{x}, \vec{\omega}_i)} = \frac{dL_o(\mathbf{x}, \vec{\omega}_o)}{L_i(\mathbf{x}, \vec{\omega}_i) \cos \theta_i d\vec{\omega}_i} \quad (3.2)$$

The BRDF states that the incoming and the outgoing radiance are proportional, so that the energy hitting the material at the point \mathbf{x} is proportional to the energy coming out from the point. BRDF functions have generally the following properties:

- *reciprocal*: for the Hemholtz reciprocity principle, a physics result that is also the basis of reverse path ray tracing [Desolneux et al., 2007]:

$$f(\mathbf{x}, \vec{\omega}_i, \vec{\omega}_o) = f(\mathbf{x}, \vec{\omega}_o, \vec{\omega}_i)$$

- *anisotropic*: if the surface changes orientation and $\vec{\omega}_i$ and $\vec{\omega}_o$ stays the same, the resulting BRDFs are different. So generally

$$f(\mathbf{x}, \vec{\omega}_i, \vec{\omega}_o) \neq f(\mathbf{x}, R\vec{\omega}_o, R\vec{\omega}_i)$$

where R is a rotation matrix with arbitrary axis around the point \mathbf{x} .

- *positive*: since BRDF regulates the transport between two positive quantities (radiance, irradiance).

$$f(\mathbf{x}, \vec{\omega}_o, \vec{\omega}_i) \geq 0$$

- *energy conserving*, so that the energy of the outgoing ray is no grater than the one of the incoming one

$$\int_{2\pi} f(\mathbf{x}, \vec{\omega}_o, \vec{\omega}_i) \cos \theta_o d\vec{\omega}_o \leq 1$$

By inverting equation 3.2, we obtain the so-called *reflectance equation*:

$$L_o(\mathbf{x}, \vec{\omega}_o) = \int_{2\pi} f(\mathbf{x}, \vec{\omega}_i, \vec{\omega}_o) L_i(\mathbf{x}, \vec{\omega}_i) \cos \theta_i d\vec{\omega}_i$$

Later we will use this equation as a starting point to obtain a formulation of the full rendering equation. The BRDF function has some limitations, being not able to account for all phenomena. For example, with a BRDF it is not possible to account for subsurface scattering, because it assumes the light enters and leaves the material at the same point. To model these phenomena, more complicated functions are needed, like the BSSRDF function described later in this chapter.

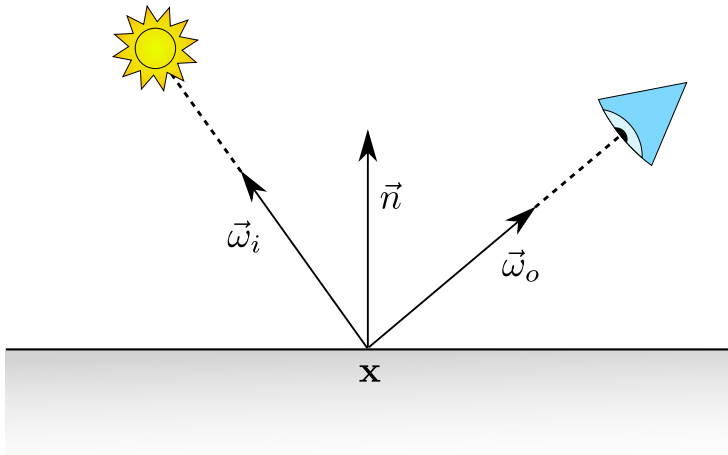


Figure 3.4: Setup for a BRDF. Note that the light enters and leaves the surface at the same point.

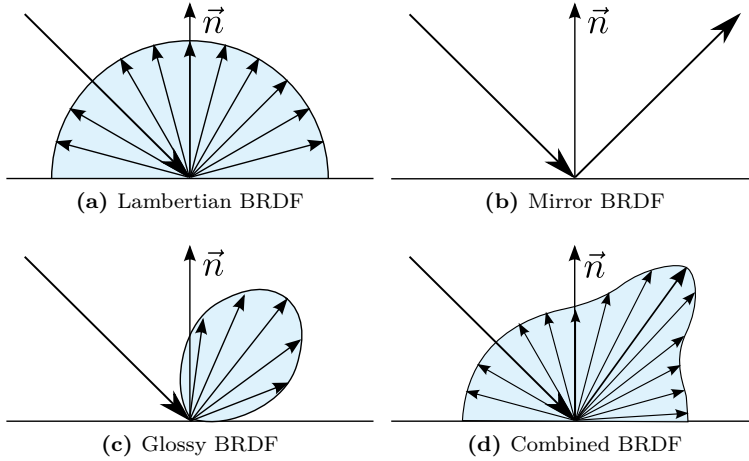


Figure 3.5: Examples of BRDF functions. In this particular example, the three simple BRDFs can be combined in the more complex BRDF of figure 3.5d in order to combine multiple effects.

3.3.2 Examples of BRDF functions

There are many examples of BRDF functions in literature. In this section, in order to illustrate some examples, we will introduce three of them: the lambertian or diffuse BRDF, the specular or mirror BRDF and glossy BRDFs. For a detailed overview on BRDF functions, please refer to [Montes and Ureña, 2012].

3.3.2.1 Lambertian BRDF

In the lambertian BRDF, the incoming radiance is distributed equally in all directions, regardless of the incoming direction. To do this, the BRDF must be constant:

$$f(\mathbf{x}, \vec{\omega}_i, \vec{\omega}_o) = k_d$$

We can check that then the radiance is scattered equally in all directions by simple integration:

$$\begin{aligned} L_o(\mathbf{x}, \vec{\omega}_o) &= \int_{2\pi} f_d L_i(\mathbf{x}, \vec{\omega}_i) \cos \theta_i d\vec{\omega}_i \\ L_o(\mathbf{x}, \vec{\omega}_o) &= k_d \int_{2\pi} L_i(\mathbf{x}, \vec{\omega}_i) \cos \theta_i d\vec{\omega}_i \\ L_o(\mathbf{x}, \vec{\omega}_o) &= k_d E(\mathbf{x}) \end{aligned}$$

The lambertian model is an ideal model, so very few material exhibit a lambertian diffusion, like unfinished wood or *spectralon*, a synthetic material created in order to be as close as possible to a perfect lambertian material. Spectralon is usually employed in calibrating radiance testing equipment.

3.3.2.2 Mirror BRDF

Another simple kind of BRDF is the perfectly specular BRDF, or mirror BRDF. In this function, all the incoming radiance from one direction $\vec{\omega}_i$ is completely diffused into the reflected direction $\vec{\omega}_r$, defined as $\vec{\omega}_r = \vec{\omega}_i - 2(\vec{\omega}_i \cdot \vec{n})\vec{n}$. The resulting BRDF is defined as follows:

$$f(\mathbf{x}, \vec{\omega}_i, \vec{\omega}_o) = \frac{\delta(\vec{\omega}_o - \vec{\omega}_r)}{\cos \theta_i}$$

The function $\delta(\vec{\omega})$ is a hemispheric delta function. Once integrated over a hemisphere, the function evaluates to one only for the vector $\vec{\omega} = \mathbf{0}$. Putting the BRDF into the reflectance equation gives the following outgoing radiance:

$$L_o(\mathbf{x}, \vec{\omega}_o) = \begin{cases} L_i(\mathbf{x}, \vec{\omega}_i) & \text{if } \vec{\omega}_o = \vec{\omega}_r \\ 0 & \text{otherwise} \end{cases}$$

that is the expected result, as all the radiance is reflected into the direction $\vec{\omega}_r$.

3.3.2.3 Glossy BRDFs

As we can see from real life experience, rarely objects are completely diffuse or completely specular. These two models are idealized models, that represent an

ideal case. So, to create a realistic BRDF model, we often need to combine the two terms and add an additional one, called glossy reflection.

The most used BRDF model used to model glossy reflections is based on microfacet theory [Ashikmin et al., 2000]. In this theory, the surface of an object is modeled as composed of small mirrors. In one of its classical formulation, the BRDF is represented as:

$$f(\mathbf{x}, \vec{\omega}_i, \vec{\omega}_o) = \frac{DGR}{4 \cos \theta_r \cos \theta_i} = \frac{GR}{4} \frac{(\vec{n} \cdot \vec{h})^s}{(\vec{n} \cdot \vec{r})(\vec{n} \cdot \vec{\omega}_i)}$$

D regulates how microfacets are distributed, and it is often modeled as $(\vec{n} \cdot \vec{h})^s$, where \vec{h} is the half vector between the eye and the light, and s is an attenuation parameter. \vec{h} is defined as:

$$\vec{h} = \frac{\vec{\omega}_o + \vec{\omega}_i}{\|\vec{\omega}_o + \vec{\omega}_i\|}$$

G accounts for the object self shadowing, while R is the Fresnel reflection term (more details in section 3.3.4). \vec{r} is the reflection vector as defined in the previous section. See figure Z on how the vectors for the glossy reflection - \vec{n} , \vec{h} and \vec{r} - are defined.

Various alternative definitions exist for the D and G function, varying among the literature. Other glossy models not based on microfacet theory do exist as well [Montes and Ureña, 2012].

3.3.3 The rendering equation

Given the reflectance equation, it is possible to generalize it in order to model all the lighting in an environment. In fact, the described reflectance equation is a suitable candidate to represent a full global illumination model, but it does not account for two important factors.

The first factor are emissive surfaces. We need to add an emissive radiance term $L_e(\mathbf{x}, \vec{\omega})$ that models the amount of radiance that a point is emitting in a certain direction. This is useful to model light sources using the same equation. Note that point lights have a singularity: they emit infinite radiance on the point they are placed.

The second factor is that the reflectance equation accounts only for direct illumination. In general, we want to model global illumination, i.e. to include also light that bounced onto another surface before reaching the current surface. To model this, we can replace the L_i term in the reflectance equation with another term L_r that accounts for light coming from another surface. This term can be usually modeled as the product of the radiance of the light plus a visibility function $V(\mathbf{x})$.

Accounting for all the described factors, we reach one formulation of the rendering equation:

$$L_o(\mathbf{x}, \vec{\omega}_o) = L_e(\mathbf{x}, \vec{\omega}) + \int_{2\pi} f(\mathbf{x}, \vec{\omega}_i, \vec{\omega}_o) L_i(\mathbf{x}, \vec{\omega}_i) V(\mathbf{x}) \cos \theta_i d\vec{\omega}_i$$

This form of the rendering equation is still not completely general, since it is based on a BRDF, so it is not possible to model subsurface scattering effects or wavelength-changing effects (like iridescence). We will extend the rendering equation in order to account for these phenomena later on in this chapter.

3.3.4 Fresnel equations

Until now, on the described BRDF models, we did consider only the reflected part of the radiance. When a beam of light coming from direction $\vec{\omega}_i$ hits a surface, only part of the incoming radiance gets reflected, while another part gets refracted into the material. As we can see from the setup from figure 3.6, we obtain the two vectors $\vec{\omega}_r$ and $\vec{\omega}_t$, the reflected and refracted vector, defined as follows:

$$\begin{aligned}\vec{\omega}_r &= \vec{\omega}_i - 2(\vec{\omega}_i \cdot \vec{n})\vec{n} \\ \vec{\omega}_t &= \eta((\vec{\omega}_i \cdot \vec{n})\vec{n} - \vec{\omega}_i) - \vec{n}\sqrt{1 - \eta^2(1 - (\vec{\omega}_i \cdot \vec{n})^2)}\end{aligned}$$

Where $\eta = \frac{n_1}{n_2}$ is the relative index of refraction of the material. With this setup, illustrated in figure 3.6, we can use a solution to Maxwell's equations for wave propagation to describe the behavior of the radiant flux. In particular, we can tell which part of the power propagates in the reflected and refracted direction respectively. The numbers that describe this division are called *Fresnel coefficients*. The coefficients are different according to the polarization of the incoming light (parallel or perpendicular), so there are two of them for the

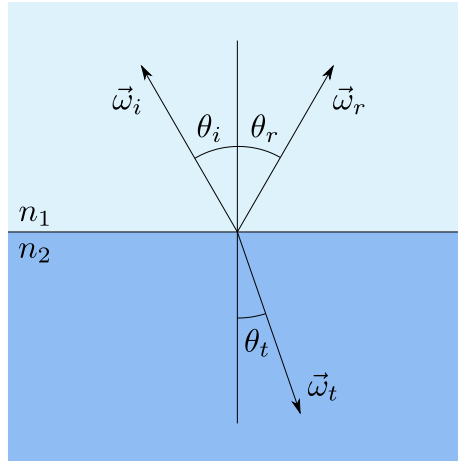


Figure 3.6: Reflected and refracted vector on mismatching indices of reflection.

reflection (R_s, R_p) and two for transmission (T_s, T_p). The coefficients relate the incoming and outgoing radiant flux of the light, and by differentiation the radiance as well.

$$\begin{aligned}
 R_s(\eta, \vec{\omega}_i) &= \left| \frac{\eta \cos \theta_i - \cos \theta_t}{\eta \cos \theta_i + \cos \theta_t} \right|^2 \\
 R_p(\eta, \vec{\omega}_i) &= \left| \frac{\eta \cos \theta_t - \cos \theta_i}{\eta \cos \theta_t + \cos \theta_i} \right|^2 \\
 T_s(\eta, \vec{\omega}_i) &= \eta \frac{\cos \theta_t}{\cos \theta_i} \left| \frac{2 \cos \theta_i}{\eta \cos \theta_i + \cos \theta_t} \right|^2 \\
 T_p(\eta, \vec{\omega}_i) &= \eta \frac{\cos \theta_t}{\cos \theta_i} \left| \frac{2 \cos \theta_i}{\eta \cos \theta_t + \cos \theta_i} \right|^2
 \end{aligned}$$

In most computer graphics applications (and this is reasonable for most of the real-world lights), we assume that the two polarizations are equally mixed. So, we will use the coefficient $R = \frac{R_s+R_p}{2}$ and $T = \frac{T_s+T_p}{2}$ in our calculations. Note that $R + T = 1$, so the overall energy is conserved.

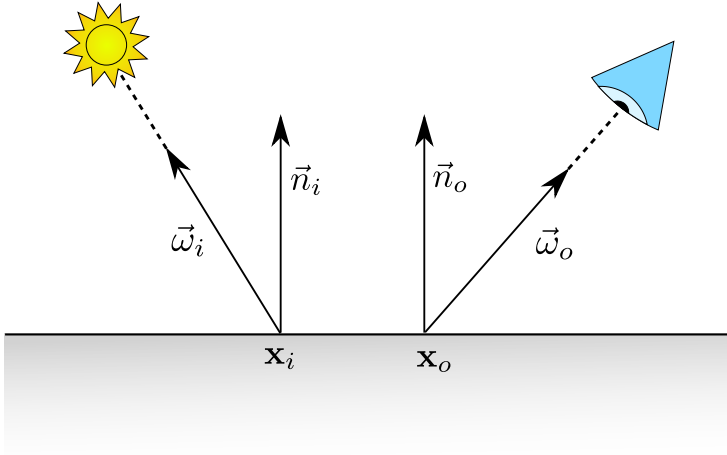


Figure 3.7: BSSRDF setup. As we compare it to the one of figure 3.4, we can see that the light enters and leaves the surface at two different points.

3.3.5 BSSRDF functions and generalized rendering equation

As we anticipated in section 3.3.1, the BRDF theory that was introduced before is not accurate in predicting the behavior in the lighting for all materials, since BRDF models assume that the light enters and leaves the material in the same point. While this assumption holds true for a wide range of material, like metal or plastic, it poorly describes translucent materials, that exhibit a consistent amount of light transport under the surface.

In order to describe light transport in this material, we introduce a function, called BSSRDF, acronym for *Bidirectional Subsurface Scattering Reflectance Distribution Function*. This function extends the concept of BRDF to account for two separate points. The BSSRDF is usually indicated with a capital S . We define the BRDF as the ratio between the incoming flux in a point \mathbf{x}_i from the direction $\vec{\omega}_i$ and the outgoing radiance in *another* point \mathbf{x}_o on direction $\vec{\omega}_o$:

$$S(\mathbf{x}_i, \vec{\omega}_i, \mathbf{x}_o, \vec{\omega}_o) = \frac{dL_o(\mathbf{x}_o, \vec{\omega}_o)}{d\Phi_i(\mathbf{x}_i, \vec{\omega}_i)} = \frac{dL_o(\mathbf{x}_o, \vec{\omega}_o)}{dE_i(\mathbf{x}_i, \vec{\omega}_i)dA_i} = \frac{dL_o(\mathbf{x}_o, \vec{\omega}_o)}{L_i(\mathbf{x}_i, \vec{\omega}_i) \cos \theta_i d\vec{\omega}_i dA_i}$$

As we can see, the BSSRDF is similar to the BRDF, apart from a additional

derivation in the area domain. Once we rearrange this equation, we can obtain an updated reflectance equation for the BSSRDF:

$$L_o(\mathbf{x}_o, \vec{\omega}_o) = \int_A \int_{2\pi} S(\mathbf{x}_i, \vec{\omega}_i, \mathbf{x}_o, \vec{\omega}_o) L_i(\mathbf{x}_i, \vec{\omega}_i) \cos \theta_i d\vec{\omega}_i dA_i$$

We can immediately see that the new reflectance equation accounts for light scattering between two points, but this generality comes with a price. In fact, it adds a order of magnitude of complexity, since now the BSSRDF needs to be integrated twice, on the whole surface and on the normal hemisphere, while the BRDF needed only once.

As we did for the BRDF, we can further extend the reflectance equation to further include visibility and emission, giving an extended form of the rendering equation.

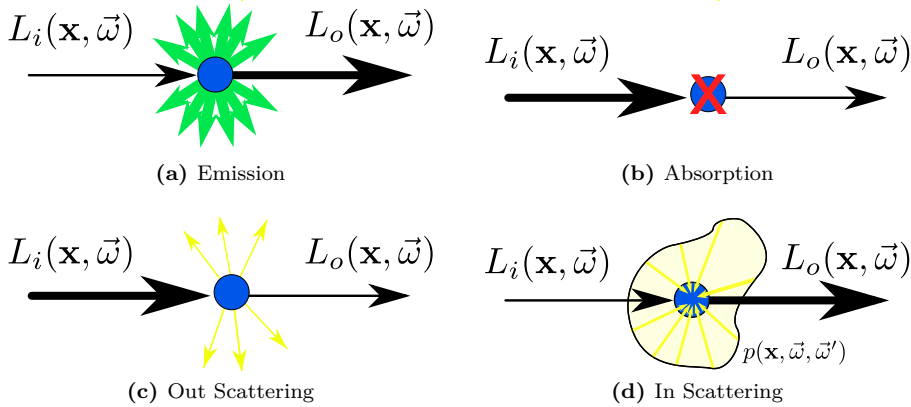
$$L_o(\mathbf{x}_o, \vec{\omega}_o) = L_e(\mathbf{x}_i, \vec{\omega}_i) + \int_A \int_{2\pi} S(\mathbf{x}_i, \vec{\omega}_i, \mathbf{x}_o, \vec{\omega}_o) L_i(\mathbf{x}_i, \vec{\omega}_i) V(\mathbf{x}) (\vec{n} \cdot \vec{\omega}_i) d\vec{\omega}_i dA_i \quad (3.3)$$

From now on, by ‘rendering equation’ in this report we will mean the one in equation 3.3.

3.4 Light transport and subsurface scattering

When we derive our models for lighting, in general we assume that the light is traveling in vacuum. This assumption holds for light that is propagating through the air (which is assimilable to vacuum), but once we relax it, more variables should be taken into consideration. Objects through which light travels are referred as *participating media*. In this chapter, we will derive and consider an alternative formulation of the rendering equation for light traveling into participating media, called *radiative transport equation*.

When a beam of light travels through an object, various phenomena occur. A photon on the beam can be either being absorbed (disappear), scattered (change direction) or emitted (appear). These phenomena can be uniform throughout the material (homogeneous materials), as in solid materials like wax or leaves, or be not uniform (heterogeneous materials), like in smoke or clouds.



We will briefly describe all three mentioned effects, then combine them to compose the radiative transport equation. The purpose is to describe how radiance varies along a beam of light with direction $\vec{\omega}$. This directional derivative is indicated as:

$$(\vec{\nabla} \cdot \vec{\omega})L(\mathbf{x}, \vec{\omega}) = \frac{\partial L_x}{\partial x}\vec{\omega}_x + \frac{\partial L_y}{\partial y}\vec{\omega}_y + \frac{\partial L_z}{\partial z}\vec{\omega}_z$$

3.4.1 Emission

Emission is the natural property of the materials to emit light, i.e. to generate photons that add to the existing ones passing through the material. The effect is generally generated by chemical processes emitting photons (as in natural animals like fireflies), by natural black-body radiation emission in the visible spectrum (such as in a star like the sun or in incandescent bulbs), or by other radiation that changes its wavelength into the visible spectrum.

In the directional 3D derivative, the variance in emission is modeled as a constant depending only on the current position and direction:

$$(\vec{\nabla} \cdot \vec{\omega})L(\mathbf{x}, \vec{\omega}) = \epsilon(\mathbf{x}, \vec{\omega})$$

This means that emission increases linearly along the body: if the beam travels a distance d within the medium, $d \cdot k$ photons are emitted. Emission is generally isotropic, not depending on the direction ($\epsilon(\mathbf{x}, \vec{\omega}) = \epsilon(\mathbf{x})$).

3.4.2 Absorption

Absorption is a property of materials that models a simple physical phenomenon: a photon, traveling though the material, hits one atom of the material. The energy carried by the photon is then absorbed by the atom, augmenting its kinetic energy. This directly translates in an increase of heat in the material. Usually, a certain percentage of the photons that hit the atoms is absorbed per unit length. Then, if k is the percentage of the photons absorbed in a meter, after one meter the original radiance will become $k \cdot L_i$, then $k^2 \cdot L_i$, etc.

If we write this phenomena as a differential equation, we get after a distance d a radiance reduction of $k^d = e^{-\sigma_a d}$, that leads to the following 3D directional derivative:

$$(\vec{\nabla} \cdot \vec{\omega})L(\mathbf{x}, \vec{\omega}) = -\sigma_a(\mathbf{x}, \vec{\omega})L(\mathbf{x}, \vec{\omega})$$

σ_a is referred as the *absorption coefficient*. Also this coefficient is generically isotropic, and constant for homogenous materials.

3.4.3 Out-scattering

Out scattering is the radiance lost due to scattering. The scattering phenomenon happens when photons are deflected away from the current direction $\vec{\omega}$. As in the previous case, the phenomena is modeled as a percentage of the radiance lost per unit length. So the loss due to out-scattering is modeled as:

$$(\vec{\nabla} \cdot \vec{\omega})L(\mathbf{x}, \vec{\omega}) = -\sigma_s(\mathbf{x}, \vec{\omega})L(\mathbf{x}, \vec{\omega})$$

σ_s is referred as the *scattering coefficient*. We note that in this case we are not interested in which direction the photons are actually going. That will be accounted in the in-scattering term of another point in the material.

3.4.4 In-scattering

Given some loss due to some of the photons changing direction, there will be some of them that from other scattering events will change to the $\vec{\omega}$ direction.

We need then to discover the number of photons that comes from all the other directions. To do this, we integrate the incoming radiance from all directions in the point \mathbf{x} . This quantity, similar to irradiance, in an infinite medium is called *fluence*, and indicated as ϕ :

$$\phi(\mathbf{x}) = \int_{4\pi} L(\mathbf{x}, \vec{\omega}') d\omega'$$

This quantity should be then averaged over the entire sphere, yielding $\frac{\phi}{4\pi}$ as a normalization factor. This quantity then is then multiplied by the scattering coefficient, because only some photons on average scatter towards the current point. This results in:

$$(\vec{\nabla} \cdot \vec{\omega}) L(\mathbf{x}, \vec{\omega}) = \sigma_s(\mathbf{x}) \frac{1}{4\pi} \int_{4\pi} L(\mathbf{x}, \vec{\omega}') d\omega' \quad (3.4)$$

However, equation 3.4 assumes that radiance scatters equally in all directions. This is not usually the case, and the $\frac{1}{4\pi}$ term needs to be replaced by a probability distribution function that describes how the photons scatter in the medium. This function is called phase function, and indicated as $p(\mathbf{x}, \vec{\omega}, \vec{\omega}')$. In the actual models its integral on the hemisphere is often used as a parameter, called *mean cosine* (g):

$$g(\mathbf{x}) = \int_{4\pi} p(\mathbf{x}, \vec{\omega}, \vec{\omega}') \vec{\omega} \cdot \vec{\omega}' d\omega'$$

This term indicates the general direction of the scattering in the material. If positive, the scattering is prevalent along the beam (forward scattering), if negative is prevalent in the opposite direction (backward scattering). If zero, the scattering is isotropic, i.e. equal in all directions.

So, the final 3D equation for in-scattering, accounting for the phase function, is as follows:

$$(\vec{\nabla} \cdot \vec{\omega}) L(\mathbf{x}, \vec{\omega}) = \sigma_s(\mathbf{x}) \int_{4\pi} p(\mathbf{x}, \vec{\omega}, \vec{\omega}') L(\mathbf{x}, \vec{\omega}') d\omega'$$

3.4.5 Final formulation of the radiative transport equation

Combining emission, absorption, scattering described in the previous sections, we reach the final formulation of the radiative transport equation (RTE):

$$(\vec{\nabla} \cdot \vec{\omega})L(\mathbf{x}, \vec{\omega}) = -\sigma_t(\mathbf{x})L(\mathbf{x}, \vec{\omega}) + \epsilon(\mathbf{x}) + \sigma_s(\mathbf{x}) \int_{4\pi} p(\mathbf{x}, \vec{\omega}, \vec{\omega}') L(\mathbf{x}, \vec{\omega}') d\omega' \quad (3.5)$$

Where the two reducing term, scattering and absorption, have been combined together in $\sigma_t = \sigma_a + \sigma_s$, called the *extinction coefficient*.

3.4.6 The diffusion approximation

The radiative transport equation 3.5 is a integro-differential equation with many degrees of freedom. As we stated in chapter 2, there are rendering techniques that numerically solve the equation in order to obtain a realistic result. However, analytical methods tend to use some approximations of the RTE, that hold well given specific conditions. The *diffusion approximation* is one of these approximations, and it is still widely used today since its introduction in the computer graphics community by Ishimaru [1997].

The assumption under the diffusion approximation is simple: given that in a physical medium there are a lot of scattering events, the beam of light quickly becomes isotropic. Each one of the scattering events blurs the light distribution, and as a result the distribution becomes more uniform as the number of scattering events increases. This has been proven to be a reasonable assumption even for highly anisotropic light sources (e.g. a focused laser beam) and phase functions.

When using the diffusion approximation, instead of using the extinction coefficient σ_t , we account for the contribution from the phase function by using the so-called *reduced extinction coefficient* σ'_t . It is defined as $\sigma'_t = \sigma_a + \sigma'_s$, with $\sigma'_s = \sigma_s(1 - g)$. σ'_s Is called *reduced scattering coefficient*. The converse of the reduced extinction coefficient is called *mean free path* and represents the average distance that light travels in the medium before being absorbed or scattered.

The rationale behind this reduced coefficient is that a highly forward scattering material is virtually indistinguishable from a not-scattering material. So, for

highly forward scattering materials ($g \approx 1$) the scattering coefficients reduces to zero. For highly backward scattering materials ($g \approx -1$), the scattering is accounted for twice as for an isotropic material (see table 3.2).

Coefficient	Backward Scattering ($g \approx -1$)	Isotropic ($g \approx 0$)	Forward Scattering ($g \approx 1$)
σ'_s	$2\sigma_s$	σ_s	0
σ'_t	$\sigma_a + 2\sigma_s$	$\sigma_a + \sigma_s$	σ_a

Table 3.2: Explicit scattering coefficients for different kinds of materials.

We leave to Ishimaru [1997] and Jensen et al. [2001] for the algebraic details of the calculation. Once we solve the diffusion equation, we obtain the following formula for $\phi(\mathbf{x})$, the fluence of light in an infinite scattering medium.

$$\phi(\mathbf{x}) = \frac{\Phi}{4\pi D} \frac{e^{\sigma_{tr} r}}{r}$$

We recall that $\phi(\mathbf{x}) = \int_{4\pi} L(\mathbf{x}, \vec{\omega}) d\vec{\omega}$. $r = \|\mathbf{x}\|$ is the distance from the point to the light source. The two coefficients D and σ_{tr} are called *diffusion coefficient* and *transmission coefficient* respectively. The two coefficients are defined as follows:

$$D = \frac{1}{3\sigma'_t}$$

$$\sigma_{tr} = \sqrt{3\sigma_a \sigma'_t} = \sqrt{\frac{\sigma_a}{D}}$$

This is the equation describe light propagation in an infinite medium, i.e. no surface interaction is considered. In order to derive an actual BSSRDF model from the diffusion approximation, *boundary conditions* must be considered. Jensen Jensen et al. [2001] derived an analytical model starting from this approximation of the RTE, while Frisvad Frisvad et al. [2013] uses a higher order diffusion approximation of the RTE. The two models are explained in the following sections.

3.4.7 Standard dipole model

The first model we describe is due to Jensen [2001]. It is usually referred in literature as *Jensen dipole model* or *Standard dipole model*. In their original paper, the authors used the diffusion approximation for light in an infinite medium. Starting from that, they derive an approximation that holds for light in a semi-infinite medium, i.e. light traveling in void hitting a planar slab of a translucent material.

As a boundary condition, we take the light coming *out* of the material. Light coming out of the material has a initial fluence ϕ_0 . We assume then that the fluence decays linearly until a distance $z = 2AD$ from the surface, where it becomes zero. See Donner [2006] for the full derivation. D is the diffusion coefficient, while A is a corrective term that accounts for materials with mismatching indices of refraction:

$$\begin{aligned} A &= \frac{1 + F_{dr}}{1 - F_{dr}} \\ F_{dr} &= \int_{2\pi} R(\eta, \vec{n} \cdot \vec{\omega})(\vec{n} \cdot \vec{\omega}) d\vec{\omega} \end{aligned} \tag{3.6}$$

Where R is the Fresnel reflection term as defined in section 3.3.4, and $\eta = n_1/n_2$ is the ratio of the refraction indices. The Fresnel reflectance integral F_{dr} is usually approximated with an analytical expression:

$$F_{dr} = -\frac{1.440}{\eta^2} + \frac{0.710}{\eta} + 0.668 + 0.0036\eta$$

Given the boundary condition, we can then model the subsurface scattering in a point \mathbf{x}_o with two small sources on the point, a configuration called a *dipole*. One source is placed beneath the surface, called the *real source*, while the other one is mirrored above the surface, called *virtual source*. The first source actually models the subsurface scattering effect, while the second one reduces the first in order to account for the boundary conditions and the extrapolation boundary. Refer to figure 3.8 for a visual detail on the setup.

The real source is placed one mean free path beneath the surface, at $z_r = 1/\sigma'_t$, while the virtual one is placed symmetrically according to the end of the boundary conditions, ad a distance $z_v = z_r + 4AD$. From z_r and z_v we

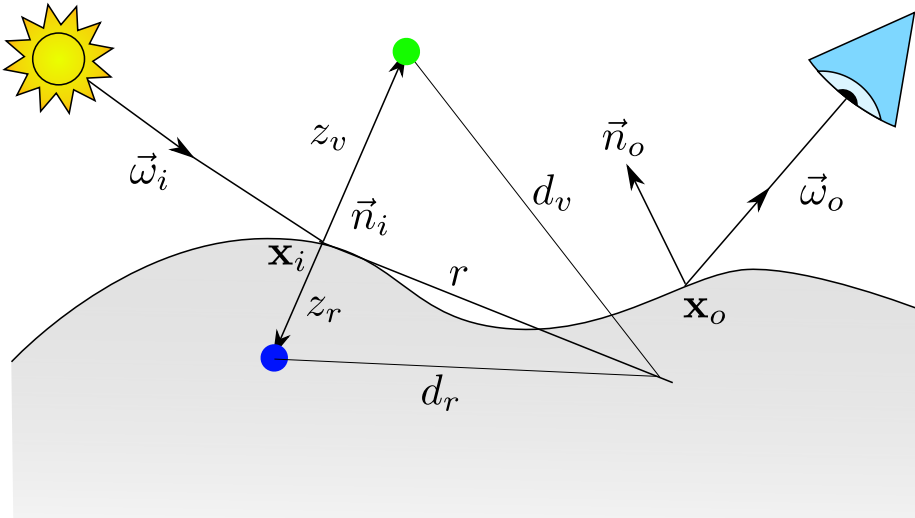


Figure 3.8: Setup for the standard dipole model.

can calculate the distances d_r and d_v from the entrance point \mathbf{x}_i . Given $r = \|\mathbf{x}_o - \mathbf{x}_i\|$, we obtain:

$$\begin{aligned} d_r &= \sqrt{z_r^2 + r^2} \\ d_v &= \sqrt{z_v^2 + r^2} \end{aligned}$$

Given these constraints, we obtain an equation for the BSSRDF in a semi infinite medium:

$$S_d(\mathbf{x}_i, \vec{\omega}_i, \mathbf{x}_i, \vec{\omega}_o) = \frac{\alpha'}{4\pi^2} \left[\frac{z_r(1 + \sigma_{tr}d_r) e^{-\sigma_{tr}d_r}}{d_r^3} + \frac{z_v(1 + \sigma_{tr}d_v) e^{-\sigma_{tr}d_v}}{d_v^3} \right]$$

Where $\alpha' = \sigma_s'/\sigma_t'$ is called *reduced albedo*.

The model so far described was intended to model only the multiple scattering BSSRDF term, S_d . In order to obtain the full BSSRDF S , a single scattering term $S^{(1)}$ must be added. Moreover, we need to add as well the two Fresnel transmission terms, one for the incoming and one for the outgoing radiance. There are in literature many approaches to model single scattering, that are out

of the scope of this report. The final BSSRDF equation for the standard dipole model then becomes:

$$S(\mathbf{x}_i, \vec{\omega}_i, \mathbf{x}_o, \vec{\omega}_o) = T(\eta, \vec{\omega}_i) S_d(\mathbf{x}_i, \vec{\omega}_i, \mathbf{x}_o, \vec{\omega}_o) T(\eta, \vec{\omega}_o) + S^{(1)}(\mathbf{x}_i, \vec{\omega}_i, \mathbf{x}_o, \vec{\omega}_o)$$

Jensen et al. [2001] in their original paper describes and justify some corrections that need to be done to the model in order to make it work with generic surfaces, and on how to account for extensions like texture support. We will not describe these extensions here, remanding to the original paper for a description.

3.4.8 Directional dipole model

Various evolution to the standard dipole model have been proposed throughout the years. In this chapter, we will introduce the BSSRDF approximation called *directional dipole*, proposed by Frisvad et al. [2013]. In the standard dipole model, in fact, the diffusive part of the BSSRDF depends only on the distance between the point of incidence and the point of emergence, that is $S_d(\mathbf{x}_i, \vec{\omega}_i, \mathbf{x}_o, \vec{\omega}_o) = S_d(\|\mathbf{x}_o - \mathbf{x}_i\|)$.

The directional dipole model, based on the diffusion approximation, accounts for the direction of the incoming light in its calculations, in order to model the scattering effects more precisely. Moreover, the model, instead of splitting the BSSRDF in a multiple and single scattering term, splits the BSSRDF into a diffusive term S_d and a term $S_{\delta E}$, called *reduced intensity*, that can be computed using the delta-Eddington approximation Joseph et al. [1976]. The final BSSRDF thus becomes:

$$S(\mathbf{x}_i, \vec{\omega}_i, \mathbf{x}_o, \vec{\omega}_o) = T(\eta, \vec{\omega}_i)(S_d(\mathbf{x}_i, \vec{\omega}_i, \mathbf{x}_o) + S_{\delta E}(\mathbf{x}_i, \vec{\omega}_i, \mathbf{x}_o, \vec{\omega}_o))T(\eta, \vec{\omega}_o)$$

Where T are the Fresnel transmission coefficients for the incoming and outgoing directions. We note also that the diffusive part of the BSSRDF does not depend on the outgoing direction $\vec{\omega}_o$.

Diffusive BSSRDF

The diffusive part of the directional dipole model uses a first-order approximation of the RTE, that for a point light in an infinite medium gives the following fluence:

$$\phi(\mathbf{x}_o, \theta) = \frac{\Phi}{4\pi D} \frac{e^{\sigma_{tr}r}}{r} \left(1 + 3D \frac{1 + \sigma_{tr}r}{r} \cos \theta \right)$$

Where D and σ_{tr} are the two scattering coefficients defined beforehand, $r = \|\mathbf{x}_o\|$ and

$$\cos \theta = \frac{\mathbf{x} \cdot \vec{\omega}_{12}}{r}$$

Where $\vec{\omega}_{12}$ is the refracted vector as defined in section 3.3.4. Comparing 3.4.8 with equation 3.4.6, we can see that we introduced a new term that depends on the angle between the refracted incoming light vector and the vector connecting incidence and emergence.

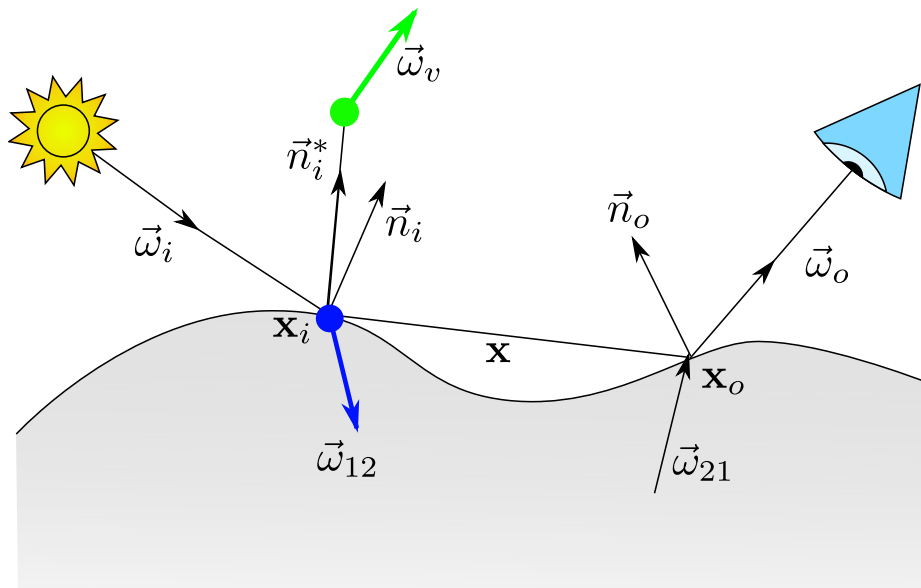


Figure 3.9: Setup for the directional dipole model.

Using the diffusion approximation, we can first establish a relationship between the radiant exitance $M(\mathbf{x}_o)$ and the diffusive BSSRDF S'_d in an infinite medium:

$$\frac{dM(\mathbf{x}_o)}{d\Phi_i(\mathbf{x}, \vec{\omega}_i)} = T(\eta, \vec{\omega}_i) S'_d(\mathbf{x}_i, \vec{\omega}_i, \mathbf{x}_o) 4\pi C_\phi(1/\eta)$$

where $C_\phi(1/\eta)$ is related to the integral on the hemisphere of the fresnel coefficients. Using the definition of radiant exitance and inserting inside the classical diffusion approximation, we reach the diffusion formulation of the radiant exitance:

$$M(\mathbf{x}_o) = C_\phi(\eta)\phi(\mathbf{x}_o) + C_{\mathbf{E}}(\eta)D\vec{n}_o \cdot \nabla\phi(\mathbf{x}_o)$$

Again, $C_\phi(\eta)$ and $C_{\mathbf{E}}(\eta)$ are two terms that are related to the integration of the fresnel coefficients. Combining the three equations TODO, we reach the final form for our diffusive BSSRDF in an infinite medium:

$$\begin{aligned} S'_d(\mathbf{x}, \vec{\omega}_{12}, r) &= \frac{1}{4C_\phi(1/\eta)} \frac{1}{4\pi^2} \frac{e^{-\sigma_{tr}r}}{r^3} \\ &\left[C_\phi(\eta) \left(\frac{r^2}{D} + 3(1 + \sigma_{tr}r)\mathbf{x} \cdot \vec{\omega}_{12} \right) - \right. \\ &- C_{\mathbf{E}}(\eta) \left(3D(1 + \sigma_{tr}r) \vec{\omega}_{12} \cdot \vec{n}_o - \right. \\ &\left. \left. - \left((1 + \sigma_{tr}r) + 3D \frac{3(1 + \sigma_{tr}r) + (\sigma_{tr}r)^2}{r^2} \mathbf{x} \cdot \vec{\omega}_{12} \right) \mathbf{x} \cdot \vec{n}_o \right) \right] \end{aligned} \quad (3.7)$$

Fresnel integrals

The two terms $C_\phi(\eta)$ and $C_{\mathbf{E}}(\eta)$ originally come from integrating the outgoing Fresnel transmittance over the whole outgoing hemisphere, weighted with a cosine term. The two functions are defined as follows:

$$\begin{aligned} C_\phi(\eta) &= \frac{1}{4\pi} \int_{2\pi} T(\eta, \vec{\omega})(\vec{n}_o \cdot \vec{\omega}) d\vec{\omega} \\ C_{\mathbf{E}}(\eta) &= \frac{3}{4\pi} \int_{2\pi} T(\eta, \vec{\omega})(\vec{n}_o \cdot \vec{\omega})^2 d\vec{\omega} \end{aligned} \quad (3.8)$$

These two integrals can be rearranged in order to express them in terms

of reflectance instead of transmittance, recalling $R = 1 - T$.

$$\begin{aligned} C_\phi(\eta) &= \frac{1}{4\pi} \left(\pi - \int_{2\pi} R(\eta, \vec{\omega}) (\vec{n}_o \cdot \vec{\omega}) d\vec{\omega} \right) = \frac{1}{4}(1 - 2C_1) \\ C_E(\eta) &= \frac{3}{4\pi} \left(\frac{2\pi}{3} - \int_{2\pi} R(\eta, \vec{\omega}) (\vec{n}_o \cdot \vec{\omega}) d\vec{\omega} \right) = \frac{1}{2}(1 - 3C_2) \end{aligned} \quad (3.9)$$

Even with this rearrangement the integral cannot be expressed in closed form. D'Eon and Irving [2011] use a convenient polynomial approximation for the two coefficients C_1 and C_2 , expressed as:

$$\begin{aligned} 2C_1 &\approx \begin{cases} +0.919317 - 3.4793\eta + 6.75335\eta^2 - 7.80989\eta^3 \\ \quad + 4.98554\eta^4 - 1.36881\eta^5 & \eta < 1 \\ -9.23372 + 22.2272\eta - 20.9292\eta^2 + 10.2291\eta^3 \\ \quad - 2.54396\eta^4 + 0.254913\eta^5 & \eta \geq 1 \end{cases} \\ 3C_2 &\approx \begin{cases} 0.828421 - 2.62051\eta + 3.36231\eta^2 - 1.95284\eta^3 \\ \quad + 0.236494\eta^4 + 0.145787\eta^5 & \eta < 1 \\ -1641.1 + \frac{135.926}{\eta^3} - \frac{656.175}{\eta^2} + \frac{1376.53}{\eta} + 1213.67\eta \\ \quad - 568.556\eta^2 + 164.798\eta^3 \\ \quad - 27.0181\eta^4 + 1.91826\eta^5 & \eta \geq 1. \end{cases} \end{aligned}$$

Boundary conditions

As the name implies, also for the directional dipole we model the boundary conditions on the material interface using a dipole. In this case, however, instead of using two point light sources, we use two ray sources, a real and a virtual one. As in the standard dipole, the source is displaced towards the normal of a distance d_e . In the case of the standard dipole, we use $2D$, that becomes $2AD$ in the case of mismatching indices of refraction on the interface. In the case of the directional dipole, we use

$$d_e = \frac{2.131D}{\sqrt{\alpha'}}$$

Where we recall $\alpha' = \sigma'_s/\sigma'_t$ as the reduced albedo. This result have been proven [Davison and Sykes, 1958] to be consistent with numerical simulations of the RTE. In addition, the A term is modified using the hemispheric Fresnel

integrals:

$$A(\eta) = \frac{1 - C_{\mathbf{E}}(\eta)}{2C_{\phi}(\eta)}$$

As the standard dipole, the directional dipole assumes a semi-infinite medium given the previous boundary conditions. In order to relax this assumptions, we need to further extend the model in order to reduce undesired effects. One first modification proposed by TODO is to use a modified tangent plane defined by the normal \vec{n}_i^* to mirror the real source towards the mirror light source, instead of the obvious one defined by \vec{n}_i . We define the modified normal as follows:

$$\vec{n}_i^* = \begin{cases} \vec{n}_i & \text{for } \mathbf{x}_o = \mathbf{x}_i \\ \frac{\mathbf{x}_o - \mathbf{x}_i}{\|\mathbf{x}_o - \mathbf{x}_i\|} \times \frac{\vec{n}_i \times (\mathbf{x}_o - \mathbf{x}_i)}{\|\vec{n}_i \times (\mathbf{x}_o - \mathbf{x}_i)\|} & \text{otherwise} \end{cases}$$

Another important modification is the distance to the real source. In the standard dipole, we used $d_r = \sqrt{z_r^2 + r^2}$, with $z_r = 1/\sigma_t'$, which is the average distance a photon travels within the material before being absorbed or scattered. The problem of this definition is that it introduces a singularity in $r = 0$. Moreover, the standard dipole becomes fairly imprecise when r is small, overestimating the overall effect. In order to avoid these problems, Frisvad et al. [2013] proposed a more complicated definition of d_r that matches simulation of transport theory more closely. For the details, see Appendix B in the original paper. d_r is defined as follows, recalling $\sigma_t = \sigma_s + \sigma_a$:

$$d_r^2 = \begin{cases} r^2 + D\mu_0(D\mu_0 - 2d_e \cos \beta) & \mu_0 \geq 0 \text{ (frontlit)} \\ r^2 + \frac{1}{(3\sigma_t)^2} & \mu_0 < 0 \text{ (backlit)} \end{cases}$$

Where $\mu_0 = -\vec{\omega}_{12} \cdot \vec{n}_o$ is an indicator if the point \mathbf{x}_o is frontlit or backlit. β is a geometry term that is evaluated as:

$$\cos \beta = -\sqrt{\frac{r^2 - (\mathbf{x} \cdot \vec{\omega}_{12})^2}{r^2 + d_e^2}}$$

Combining all the corrections seen so far, we can write the final form of our BSSRDF model, that is a combination of the real source term minus the virtual source term:

$$S_d(\mathbf{x}_i, \vec{\omega}_i, \mathbf{x}_o) = S'_d(\mathbf{x}_o - \mathbf{x}_i, \vec{\omega}_{12}, d_r) - S'_d(\mathbf{x}_o - \mathbf{x}_v, \vec{\omega}_v, d_v)$$

Where the extra coefficients are defined as follows:

$$\begin{aligned}x_v &= x_i + 2Ad_e\vec{n}_i^* \\ \vec{\omega}_v &= \vec{\omega}_{12} - 2(\vec{\omega}_{12} \cdot \vec{n}_i^*)\vec{n}_i^* \\ d_v &= \|x_o - x_v\|\end{aligned}$$

The directional dipole model described in this chapter, gives a better result than the standard dipole, at the extra price of additional calculations. In particular, the model improves the previous one for highly forward scattering materials, where it is sensibly closer to the path traced result. The final goal of this thesis is to provide a real-time implementation of it. Given this theoretical introduction, in the next section we will describe our contribution in order to breakdown the problems and the issues of a real-time implementation.

CHAPTER 4

Method

In this chapter, after giving the theoretical foundations in the topic of this report, we introduce our method to render translucent materials efficiently using the directional dipole. This chapter is meant to connect the theory presented in the last chapter with the implementation. First of all, we will start this chapter with a list of constraints and assumptions in order to better define the scope of our method. Secondly, we will give a theoretical justification of our method, deriving a discretization of the rendering equation that can be actually solved and implemented in a GPU environment. Then, we will discuss some possible sampling patterns and how they could possibly improve the results of the final rendering. Then, we will introduce how the actual scattering parameters are acquired in an experimental environment, in order to obtain a plausible result. Finally, we will describe a method to approximate environment lighting using an arbitrary number of directional sources.

4.1 Constraints and assumptions

Before describing the actual method, we will introduce some constraints and assumptions on our method. Some of these assumptions and constraints are well known to the graphics community, and they are generally introduced to

allow better performance, quality and flexibility. Being a real-time rendering method implies that performance plays a big part in the decisions made in the process, but since the method uses a physically based approximation the final quality of the result is also important. In the process the aspect of flexibility has been taken into account: the tradeoff between quality and performance should be tweakable with the fewest number of variables as possible. We will now list the assumptions we made in all the three described domains, quality, performance and flexibility, in order to later justify our method in the light of these assumptions.

4.1.1 Quality constraints

1. Being close as much as possible to a path traced solution. By *close* we mean that the root mean square of the comparison between our method and a path traced result under the same lighting conditions should not be over a certain threshold.
2. Being consistent with the directional dipole model for a wide range of material properties. In particular, the method should perform well in the domain of quality where the directional dipole model excels (highly scattering materials).
3. Being potentially able to render an object under an arbitrary number of directional sources, point light sources and one environment map.

4.1.2 Flexibility requirements

1. Work with the less amount as possible of provided model data, i.e. only the position data and eventually the normals should be provided in order for the method to run. In particular, no unwrap of the mesh (UV mapping) should be necessary. In case normal data are missing, being able to generate them using a standard method to give a smooth appearance.
2. Be possible to be integrated in a game engine environment, using data from other computations (e.g. from other lighting computations or from other techniques such as shadow mapping) and being adaptable to different lighting paths (forward and deferred shading).
3. The quality versus performance tradeoff should be set by a potential artist or developer, with the fewest number of parameters as possible.

4.1.3 Performance requirements

1. Being real-time on a high-end modern GPU, i.e. one frame should take less than 100 ms (10 FPS) to render. The ideal result would be to reach a rendering time of less than 16 ms (60 FPS).
2. Being as less dependent as possible from the geometrical complexity of the model.
3. Being as less as dependent from the viewport resolution.
4. If the desired quality is not reachable within one frame, converge towards a result in a reasonable amount of time. Techniques should be used to approximate the required quality for the intermediate result.
5. Maintain a reasonable performance under changing light conditions, deformations and change of parameters, with little or none performance penalties.
6. Employ the advantages of the directional dipole model to improve performance.
7. Support a certain number of directional and point lights (up to 3 to 5 pixel lights, as in commercial engines[Unity, 2012]).
8. Require little or no pre-processing in order to be able to perform. In particular, pre-processing, if any, should be general and performed only at the beginning of the life cycle of the program.
9. Employ and explore the latest features in the available graphics drivers and libraries. The details on which feature will be used are left to the implementation section.

4.2 Method overview

First of all, we recall the general form of the rendering equation for participating media using a BSSRDF (equation 3.3):

$$L_o(\mathbf{x}_o, \vec{\omega}_o) = L_e(\mathbf{x}_i, \vec{\omega}_i) + \int_A \int_{2\pi} S(\mathbf{x}_i, \vec{\omega}_i, \mathbf{x}_o, \vec{\omega}_o) L_i(\mathbf{x}_i, \vec{\omega}_i) V(\mathbf{x}_i) (\vec{n}_i \cdot \vec{\omega}_i) d\vec{\omega}_i dA_i$$

In the usual approach to offline path traced rendering, for each pixel of the final image we need to integrate the radiance from all the possible sources on the surface point seen by the pixel. For this surface element subtended by one pixel, all the incoming radiance contributions from the other points in the scene must be accounted and then multiplied by the BSSRDF function in the direction of the camera. In a way, we are basically performing the integral in equation 3.3 numerically. If we use a BSSRDF function, the contribution from all the points from the other surfaces must be employed, while in the case of a BRDF some contribution may be excluded (e.g., if there is an opaque surface between two points). Given its natural exponential explosion, path tracing is not obviously suitable for real-time rendering.

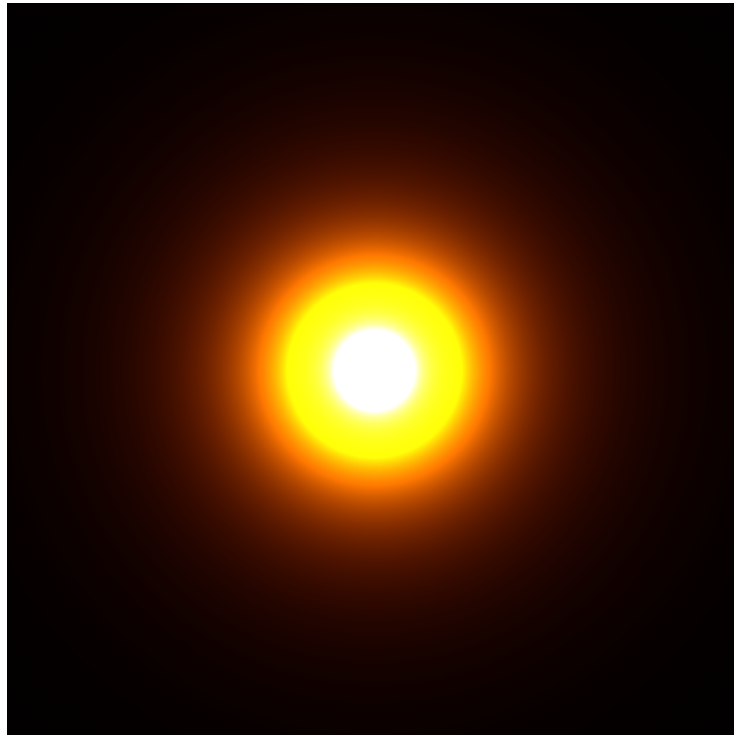


Figure 4.1: Simulation of the BSSRDF of a laser hitting a slab of 2x2 cm of potato material. We note the exponential decay of the subsurface scattering phenomena.

In our method, in its final goal to be real time, we perform the same integral as equation 3.3, but under some assumptions and restrictions that allow us to perform it more efficiently. In addition, since our method approximates the *integral* and not the BSSRDF function, it is applicable to any BSSRDF function,

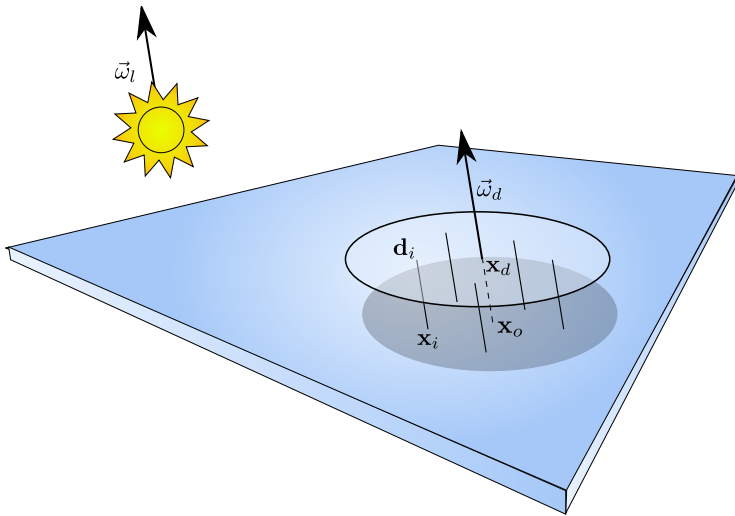


Figure 4.2: Setup for our method: the disk is placed on the point \mathbf{x}_o , displaced along the disc direction $\vec{\omega}_d$ and then the sample points \mathbf{d}_i are reprojected back to find the samples \mathbf{x}_i .

given that it has limited or no dependence on the outgoing direction $\vec{\omega}_o$, like the directional dipole model.

The idea on approximating the integral comes from the fact that the directional dipole (and subsurface scattering effects) generally decay exponentially from the point of incidence, as we can see from figure 4.1; where we show the simulation of a laser light hitting a surface in one point. So, the subsurface scattering contribution for points that are far apart becomes quickly negligible. The distance on which these effects become negligible is usually related to the transmission coefficient σ_{tr} . We will investigate this relation better in the result section.

So, given this exponential decay, we place a sample disc on the surface for a position \mathbf{x}_o . We define a sampling disc as a point \mathbf{x}_d , a radius r_d and a direction $\vec{\omega}_d$. From this disc, we chose a subset of surface points, called *sample points*. To get these points, we project the points from the disc \mathbf{d}_i on the surface M , using the disc normals as a direction (see figure 4.2 for an illustration of the process). In formulas, we do:

$$\mathbf{x}_i = \mathbf{d}_i - s\vec{\omega}_d, s \in \mathbb{R}, \mathbf{x}_i \in M$$

Then, we calculate and average the BSSRDF contribution from these points \mathbf{x}_i^k

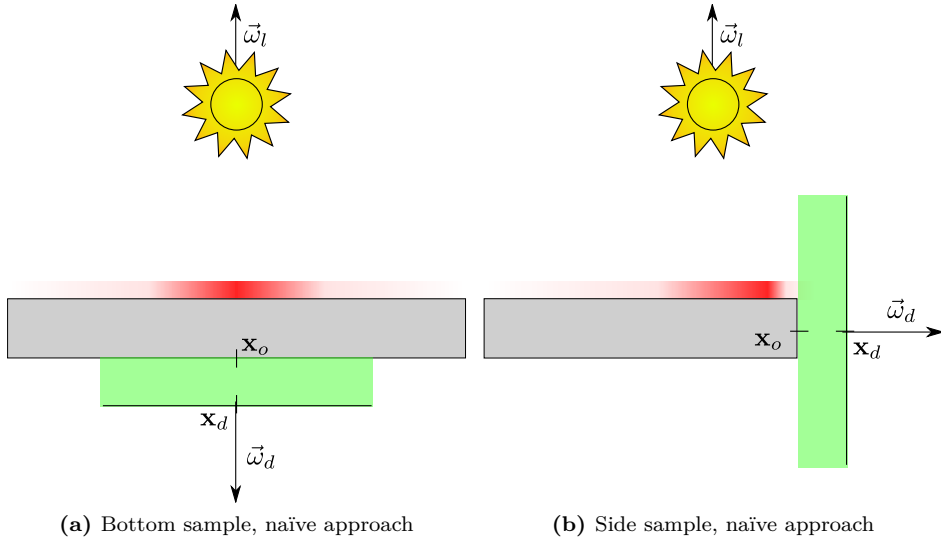


Figure 4.3: Counter examples of the naïve choice for \mathbf{x}_d and $\vec{\omega}_d$. The green area represent the sampling area of the disc (see from the side). The red area shows where on the surface the contribution is higher for the point \mathbf{x}_o . We can see that with this approach all the contribution is actually missed.

on the point x_o . The process can be repeated more times for multiple lights, using the same sampling points.

Given this set up, we need to find a way of efficiently placing the disc in order to get a good approximation of the BSSRDF. In fact, if the disc is placed in the wrong position, the accounted contribution from the sampling points will not be correct. Moreover, also the orientation of the disc is important, in order to not undersample light in certain regions of the model. A naïve approach would suggest to pick $\mathbf{x}_d = \mathbf{x}_o$ and $\vec{\omega}_d = \vec{n}_o$, but we can see that this approach is not correct. The most obvious counter examples are displayed in Figure 4.3: in the first example 4.3a, the contribution from the surrounding points will be zero, because none of the sampling points is directly illuminated by the light, so the visibility term on the rendering equation will evaluate to zero. In the second example (figure 4.3b), the wrong direction \vec{n}_o prevents the most of the points from being sampled.

A more careful choice for placing the points in the disc is to place the disc in a way that the obtained surface point is always the closest one to the light. To ensure that the points \mathbf{x}_i always have this property, we can place \mathbf{x}_d far enough

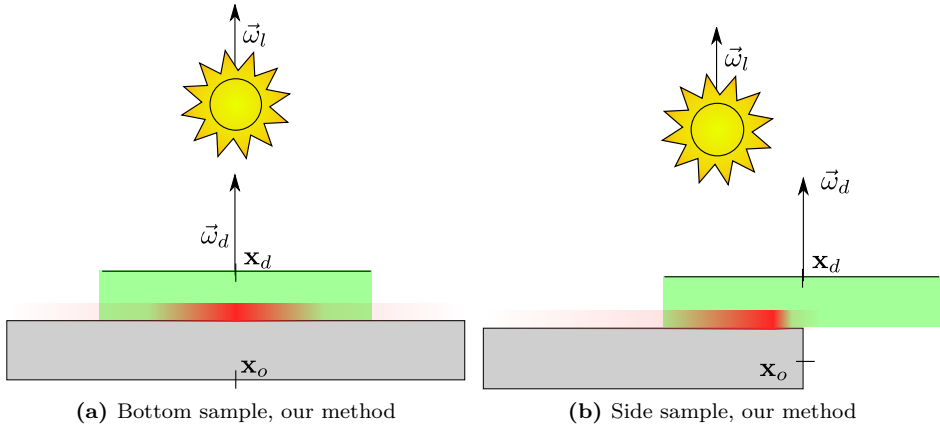


Figure 4.4: The counter examples of figure 4.3 updated using our method of choice for \mathbf{x}_d . We can see that now most of the radiance distribution is accounted for.

from the surface in a way that all the sampling points have to be the closest to the light. If we define a *bounding box vector* in the same coordinate frames, we have a simple formulation for \mathbf{x}_d :

$$\mathbf{x}_d = \mathbf{x}_o + (\mathbf{b} \cdot \vec{\omega}_l) \vec{\omega}_l$$

The bounding box vector is a vector where its components are the maximum extension of the mesh in the coordinate reference system. So,

$$\mathbf{b} = (\max(\mathbf{x}_i^x) - \min(\mathbf{x}_i^x), \max(\mathbf{x}_i^y) - \min(\mathbf{x}_i^y), \max(\mathbf{x}_i^z) - \min(\mathbf{x}_i^z)), \quad \forall \mathbf{x}_i$$

To solve the problem in the second example in figure 4.3b, we chose to always orient the circle towards the light, that is $\vec{\omega}_d = \vec{\omega}_l$ for directional lights and $\vec{\omega} = \frac{\mathbf{x}_l - \mathbf{x}_d}{\|\mathbf{x}_l - \mathbf{x}_d\|}$ for point lights. As we can see, for the new choices of disc placement and orientation we are able to catch the points from where the contribution is stronger. This new setup seems much more complicated than the naïve approach, but as we will see in the implementation section the Z-buffer of the GPU will permit us to get the desired point without any additional computation.

For environment lights, we will see how to transform them in directional lights at the end of this chapter, so the setup of the equations will be the same for directional lights.

4.2.1 Approximation of the rendering equation

Going into the mathematical details the idea is to take the integral form of the rendering equation (equation 3.3):

$$L_o(\mathbf{x}_o, \vec{\omega}_o) = L_e(\mathbf{x}_i, \vec{\omega}_i) + \int_A \int_{2\pi} S(\mathbf{x}_i, \vec{\omega}_i, \mathbf{x}_o, \vec{\omega}_o) L_i(\mathbf{x}_i, \vec{\omega}_i) V(\mathbf{x}_i) (\vec{n}_i \cdot \vec{\omega}_i) d\vec{\omega}_i dA_i$$

First of all, we make the assumption of a body that is not emitting light: all the radiance from the body comes from an external source. This assumption can be trivially relaxed and implemented, but to simplify the equation in this chapter we will exclude it from the calculations. Secondly, we limit ourselves to the case of one directional light, treating the case of a point light later as an extension. The directional light direction $\vec{\omega}_l$ and radiance $L_d \delta(\vec{\omega}_d)$.

Under the first assumption, equation 3.3 becomes:

$$\begin{aligned} L_o^D(\mathbf{x}_o, \vec{\omega}_o) &= \int_A \int_{2\pi} S(\mathbf{x}_i, \vec{\omega}_i, \mathbf{x}_o, \vec{\omega}_o) L_d \delta(\vec{\omega}_l) V(\mathbf{x}_i) (\vec{n}_i \cdot \vec{\omega}_i) d\vec{\omega}_i dA_i \\ L_o^D(\mathbf{x}_o, \vec{\omega}_o) &= \int_A S(\mathbf{x}_i, \vec{\omega}_l, \mathbf{x}_o, \vec{\omega}_o) L_d V(\mathbf{x}_i) (\vec{n}_i \cdot \vec{\omega}_l) dA_i \end{aligned}$$

In this way, we remove the internal integral. Then, in order to make a computable calculation, we need to discretize the remaining integral. We imagine to have a set of N points on the surface. We assume that each one of these points is visible from the light source (so we can get rid of the $V(\mathbf{x}_i)$ term). We will discuss in the implementation section how to make sure that all these points are visible. Each one of these points has an associated area A_i , so that we can write:

$$L_o^D(\mathbf{x}_o, \vec{\omega}_o) = L_d \sum_{i=1}^N S(\mathbf{x}_i, \vec{\omega}_l, \mathbf{x}_o, \vec{\omega}_o) (\vec{n}_i \cdot \vec{\omega}_l) A_i \quad (4.1)$$

Now, instead of using all the points on the surface, we consider only the points within a certain radius r^* from the point \mathbf{x}_o , i.e. the disk we discussed in the previous section. Assuming the points are distributed uniformly on the disk, we obtain the following area for a point:

$$A_i = \frac{A_c}{N (\vec{n}_i \cdot \vec{\omega}_l)}$$

Where $A_c = \pi(r^*)^2$ is the area of the circle. Inserting into equation 4.1, we obtain:

$$L_o^D(\mathbf{x}_o, \vec{\omega}_o) = L_d \frac{A_c}{N} \sum_{i=1}^N S(\mathbf{x}_i, \vec{\omega}_l, \mathbf{x}_o, \vec{\omega}_o) \quad (4.2)$$

That is our final approximation for a directional light. For a point light, following the exact same steps, we reach a similar solution. We recall that a point light is defined by an intensity I_p and a source point \mathbf{x}_p :

$$L_o^P(\mathbf{x}_o, \vec{\omega}_o) = I_p \frac{A_c}{N} \sum_{i=1}^N \frac{S(\mathbf{x}_i, \frac{\mathbf{x}_p - \mathbf{x}_i}{\|\mathbf{x}_p - \mathbf{x}_i\|}, \mathbf{x}_o, \vec{\omega}_o)}{\|\mathbf{x}_p - \mathbf{x}_i\|^2} \quad (4.3)$$

And, since the radiance is linearly summable, we can combine the contribution from an arbitrary number of $P_1, P_2 \dots P_p$ point sources and $D_1, D_2 \dots D_d$ directional sources:

$$\begin{aligned} L_o(\mathbf{x}_o, \vec{\omega}_o) &= \\ &= \sum_{k=1}^p L_o^{P_k}(\mathbf{x}_o, \vec{\omega}_o) + \sum_{k=1}^d L_o^{D_k}(\mathbf{x}_o, \vec{\omega}_o) \\ &= \frac{A_c}{N} \left[\sum_{k=1}^p I_p^k \sum_{i=1}^N \frac{S(\mathbf{x}_i, \frac{\mathbf{x}_p^k - \mathbf{x}_i}{\|\mathbf{x}_p^k - \mathbf{x}_i\|}, \mathbf{x}_o, \vec{\omega}_o)}{\|\mathbf{x}_p^k - \mathbf{x}_i\|^2} + \sum_{k=1}^d L_d^k \sum_{i=1}^N S(\mathbf{x}_i, \vec{\omega}_l^k, \mathbf{x}_o, \vec{\omega}_o) \right] \end{aligned} \quad (4.4)$$

4.3 Sampling patterns

As we discussed, the BSSRDF function for the directional dipole is dominated by an exponential decay. So, it is more probable to find points that contribute more to the BSSRDF if we take points closer to the evaluation point \mathbf{x}_o . However, our assumption of uniform areas in the previous calculations does not hold

anymore, so we need to modify the previous equations in order to account for the non-linear sampling.

Assuming to have a number generator that can generate numbers on a disc, we can create an exponentially distributed disc with the following exponential probability distribution function (PDF):

$$pdf(x) = \sigma_{tr} e^{-\sigma_{tr}x}$$

The difference between a disc sampled using this distribution and an uniform one is shown in figure 4.5. The process to create this distribution will be illustrated in the implementation section, assuming for now to have already obtained one. The radius of the point \mathbf{x}_i is:

$$r_i = \|\mathbf{x}_o^{proj} - \mathbf{x}_i^{proj}\|$$

Where the two points have been projected on the circle. So now we have a new normalization term to include in order to scale back the result. So, we need now to divide by a $\exp(-\sigma_{tr}r_i)$ term each sample. The new equation for a directional light then becomes:

$$\hat{L}_o^D(\mathbf{x}_o, \vec{\omega}_o) = L_d \frac{A_c}{N} \sum_{i=1}^N S(\mathbf{x}_i, \vec{\omega}_l, \mathbf{x}_o, \vec{\omega}_o) e^{\sigma_{tr}r_i}$$

The other two equations 4.2 and 4.2 then change accordingly:

$$\hat{L}_o^P(\mathbf{x}_o, \vec{\omega}_o) = I_p \frac{A_c}{N} \sum_{i=1}^N \frac{S(\mathbf{x}_i, \frac{\mathbf{x}_p - \mathbf{x}_i}{\|\mathbf{x}_p - \mathbf{x}_i\|}, \mathbf{x}_o, \vec{\omega}_o)}{\|\mathbf{x}_p - \mathbf{x}_i\|^2} e^{\sigma_{tr}r_i}$$

$$\begin{aligned} \hat{L}_o(\mathbf{x}_o, \vec{\omega}_o) &= \\ &= \sum_{k=1}^p \hat{L}_o^{P_k}(\mathbf{x}_o, \vec{\omega}_o) + \sum_{k=1}^d \hat{L}_o^{D_k}(\mathbf{x}_o, \vec{\omega}_o) \\ &= \frac{A_c}{N} \left[\sum_{k=1}^p I_p^k \sum_{i=1}^N \frac{S(\mathbf{x}_i, \frac{\mathbf{x}_p^k - \mathbf{x}_i}{\|\mathbf{x}_p^k - \mathbf{x}_i\|}, \mathbf{x}_o, \vec{\omega}_o)}{\|\mathbf{x}_p^k - \mathbf{x}_i\|^2} e^{\sigma_{tr}r_i} + \sum_{k=1}^d L_d^k \sum_{i=1}^N S(\mathbf{x}_i, \vec{\omega}_l^k, \mathbf{x}_o, \vec{\omega}_o) e^{\sigma_{tr}r_i} \right] \end{aligned}$$

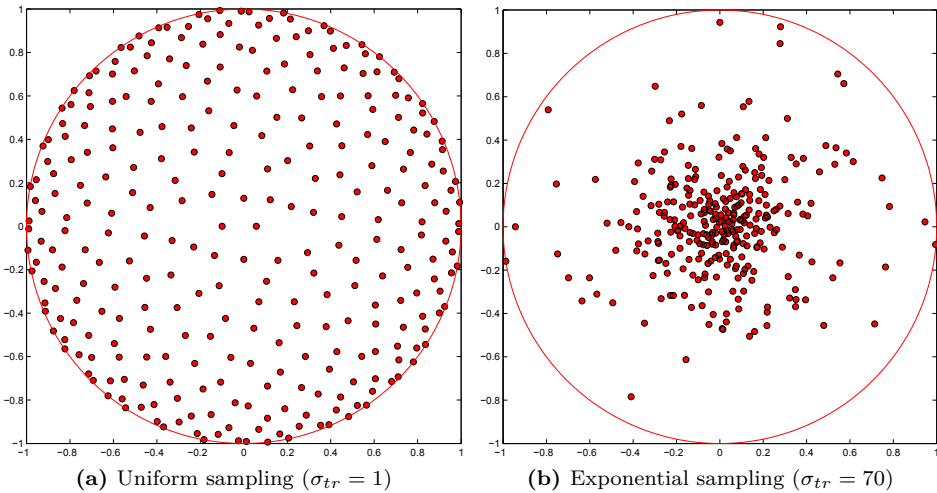


Figure 4.5: Uniform versus exponentially-weighted sampling of 300 points.

4.4 Parameter acquisition

When rendering translucent materials, it is important that we have the right scattering properties, in order to match the appearance of real world objects. The scattering parameters may be tweaked by the artist and set up manually, but this is a long process since the scattering properties are not directly related to material appearance. In order to avoid this problems, the scattering parameters are measured from samples taken from real world objects. In this section, we will give an overview of two methods used to estimate the scattering parameters.

The first method was presented alongside the standard dipole model by Jensen et al. [2001]. The measurement apparatus consists of a series of lenses that focus the light on the sample. The light power Φ is measured by calibrating the sensor with a spectralon sample. A picture of the sample is then acquired at different exposure, in order to build an high dynamic range image. This is necessary since the scattering decays exponentially, so a high range is needed to have meaningful measurements. The measured data are then fitted to diffusion theory in order to obtain the scattering coefficients. Due to the nature of the measurement, it is not possible to measure the mean cosine g of the material, but only the reduced scattering coefficient $\sigma'_s = \sigma_s(1 - g)$ and the absorption coefficient σ_a . This measurement model uses the diffusion approximation to work, so it shares the same limitations: it is valid only for materials where $\sigma_a \ll \sigma_s$.

The second method, proposed by Narasimhan et al. [2006] proposes a method to measure the scattering coefficient by dilution. The assumption is that water does not interfere with the scattering properties of the materials dissolved within it for small distances (less than 50 cm). Naturally, the material needs then to be already in a liquid form, or to be a powder that can be easily dissolved in water. The setup of the experiment is a box full of water with a camera and an area light. High dynamic range picture of the material dissolved in water are then taken, and the scattering coefficients can be measured with a low error. Various measurements at different concentrations are needed in order to get an effective measurement of the coefficients, but then the coefficients can be extrapolated for any concentration.

Some of the scattering properties measured thanks to this method are reported in table 4.1. This coefficients will be used throughout the report when referencing to a specific material.

Material	Absorption, σ_a			Scattering, σ_s			Mean cosine, g			η	Source
	R	G	B	R	G	B	R	G	B		
Apple	0.0030	0.0034	0.0046	2.29	2.39	1.97	-	-	-	1.3	J
Ketchup	0.061	0.97	1.45	0.18	0.07	0.03	-	-	-	1.3	J
Marble	0.0021	0.0041	0.0071	2.19	2.62	3.00	-	-	-	1.5	J
Potato	0.0024	0.0090	0.12	0.68	0.70	0.55	-	-	-	1.3	J
Whole milk	0.0011	0.0024	0.014	2.55	3.21	3.77	-	-	-	1.3	J
Coffee	0.1669	0.2287	0.3078	0.2707	0.2828	0.297	0.907	0.896	0.88	1.3	N
Soy milk	0.0001	0.0005	0.0034	0.2433	0.2714	0.4563	0.873	0.858	0.832	1.3	N
Wine (merlot)	0.7586	1.6429	1.9196	0.0053	0	0	0.974	0	0	1.3	N
Beer (Budweiser)	0.1449	0.3141	0.7286	0.0037	0.0069	0.0074	0.917	0.956	0.982	1.3	N
White grapefruit juice	0.0096	0.0131	0.0395	0.3513	0.3669	0.5237	0.548	0.545	0.565	1.3	N

Table 4.1: Scattering material parameters estimated using different methods. For the source field, J materials come from Jensen et al. [2001], while N materials come from Narasimhan et al. [2006]. Note that the materials measured with the technique proposed in Jensen et al. [2001] are without the g coefficient.

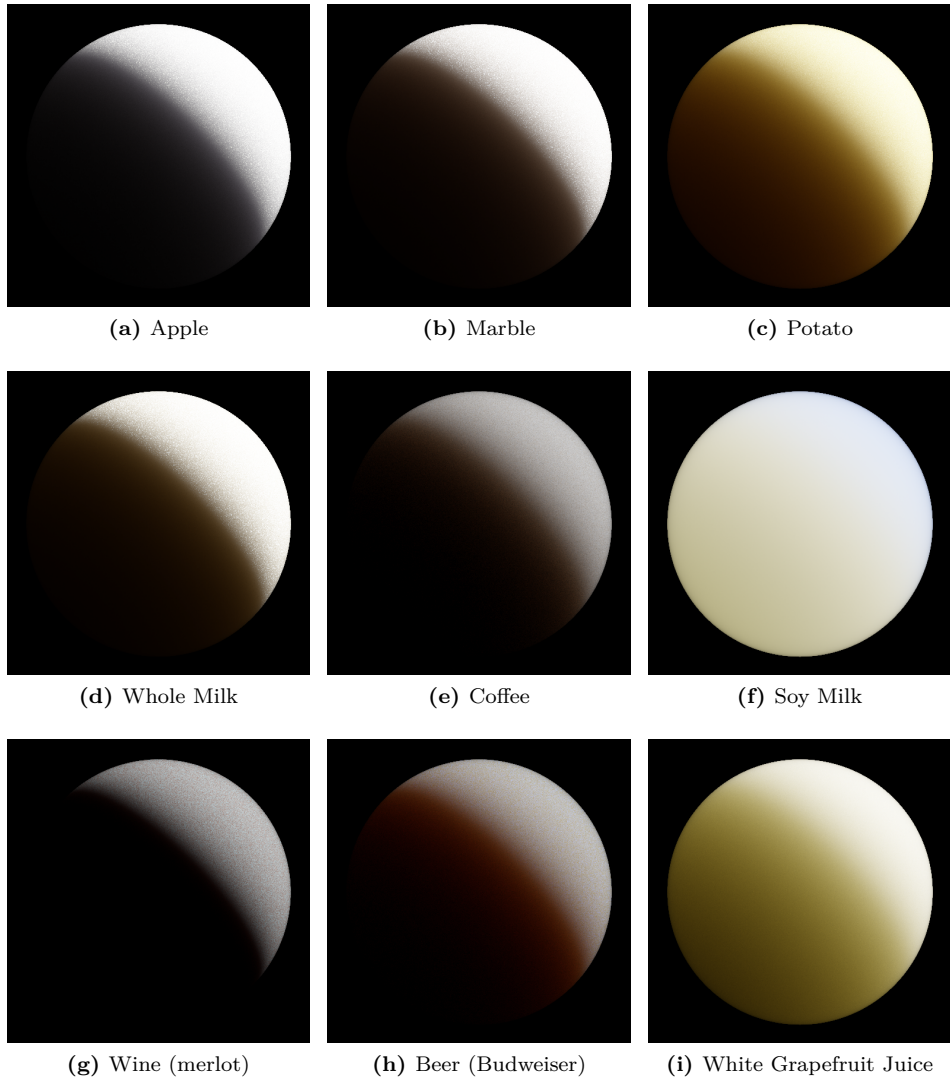


Figure 4.6: Path traced rendering on a sphere of the materials described in table 4.1.

4.5 Environment lights

Environment lighting is a omni-directional lighting that represents lighting coming from an environment. Instead of defining a light as a direction or a point in space, we define directly the radiance distribution on a map. The map is usually provided in a HDR format in order to cover various range of radiance, and it is usually given as a set of six cube faces (cubemap) or as a latitude-longitude map, as the one in figure 4.7. The maps are usually given in equirectangular projection.

In the game development community, spherical harmonics (SH) [Green, 2003, Sloan, 2008] are usually employed. This technique, given an heavy pre-computation step, transforms the radiance map into a set of coefficients in the spherical harmonics basis. This coefficients that then can be used easily to represent the radiance map, if we are interested only in the low-frequency part of it.



Figure 4.7: Latitude - longitude environment map of the inner courtyard of the Doge's palace in Venice (Doge map). The map has been converted to a RGB format from the original HDR format. Image courtesy of <http://gl.ict.usc.edu/Data/HighResProbes/>.

In this chapter, we introduce a technique presented in Pharr and Humphreys [2004] to convert a environment map into a set of directional light sources of arbitrary size. The general idea is to generate a set of random points and them transform them according to a pre-computed probability distribution. This distribution make the random point concentrate in areas where the radiance is higher, so that it is possible to get the most representative points on the radiance map. The found points are then transformed into a spherical coordinate basis

in order to get the light direction.

We start defining our image as an array of n rows and m columns. We need to define a function that of each pixel of the image gives us a single radiance value. Instead of using radiance, we use luminance. The ITU-R recommendation standard BT.709[ITU, 2001] gives us a formula to obtain luminance from spectral radiance values:

$$f(u, v) = 0.2126 R(u, v) + 0.7152 G(u, v) + 0.0722 B(u, v)$$

Where $[u, v] \in [0, n) \times [0, m)$. R , G and B represent the spectral coordinates of the radiance map. We would like to define now a probability distribution function based on the $f(u, v)$ function. We can define it simply by normalizing f with the integral of the function over the domain:

$$p(u, v) = \frac{f(u, v)}{\iint f(u, v) dudv} = \frac{f(u, v)}{\sum_u \sum_v f(u, v)}$$

However, in order to be able to sample from the distribution $p(u, v)$, there are some things to take care about. We would like now to separate the two variables, in order to sample from two one-dimensional distribution, instead of one two-dimensional distribution. To do this, we use the conditional probability formula:

$$p(u, v) = p_v(v|u)p_u(u)$$

So that we first choose u , sample its probability $p_u(u)$ and then compute the conditional density $p_v(v|u)$ using the found value for u . Using the marginal formulas, the first probability is easily found:

$$p_u(u) = \int p(u, v) dv = \frac{\sum_v f(u, v)}{\sum_u \sum_v f(u, v)}$$

And, from equation 4.5, we find the conditional probability:

$$p_v(v|u) = \frac{p(u, v)}{p_u(u)} = \frac{f(u, v)}{\sum_v f(u, v)} \sin \theta$$

The $\sin \theta$ comes from the fact that the latitude-longitude map with a equirectangular projection is not area preserving. So, the sampling must take into account the distortion of the map, otherwise the samples will be more concentrated at the poles, rather than distributed uniformly on the sphere. We can appreciate the difference for a random sampling on a sphere in figure 4.8.

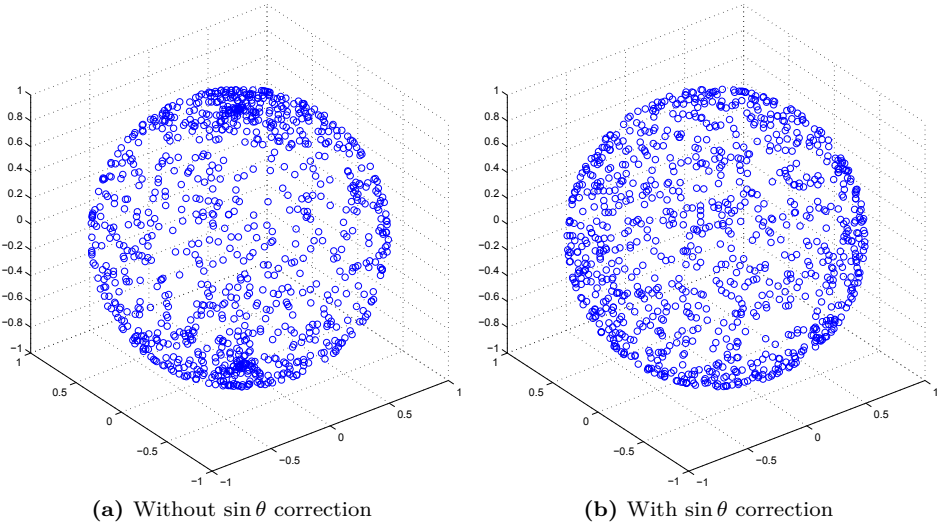


Figure 4.8: Effect of $\sin \theta$ on a random point distribution on a sphere.

Now we are ready to sample the function. In order to bias our sample according to the radiance distribution, we need to calculate the cumulative distribution function (CDF) for a one-dimensional probability distribution function. The CDF is defined as:

$$c_u(u) = \int_{-\infty}^u p_u(u) du = \sum_{i=0}^u p_u(u)$$

That is the discrete integral of the function up to the point u . Figure 4.9 explain why. If, as the figure, all the radiance is distributed towards the right side of the picture (i.e. the CDF rises slowly), if we pick a set of random points and

reverse the CDF on them, we obtain a new set of points that is biased towards the highest concentration of radiance.

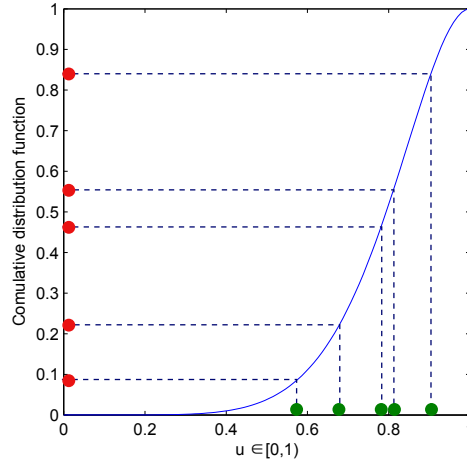


Figure 4.9: Effect of weighting values with the CDF. We note that the random values on the y axis are transformed and accumulated where the CDF is steeper.

Let us now pick a couple of random points $(\zeta_1, \zeta_2) \in [0, 1]^2$. We then convert these points to a pair of coordinates $(u_b, v_b) \in [0, n] \times [0, m]$ by inverse sampling of the CDF. We will give the details of how to discretize this process in the implementation section. Then, we obtain the spherical coordinates using the standard formula:

$$(\theta, \phi) = \left(\frac{u_b}{\pi n}, \frac{v_b}{2\pi m} \right)$$

And, from the spherical coordinates, we use the equirectangular projection formula to transform them into a vector in the 3D space, that is the final direction for our light.

$$\vec{\omega}_l = (\cos \phi \sin \theta, \sin \phi \sin \theta, \cos \theta)$$

And, by varying the random values (ζ_1, ζ_2) , obtain a set of directions that we can use for rendering. The generated points for the Doge map can be seen in figure 4.10.

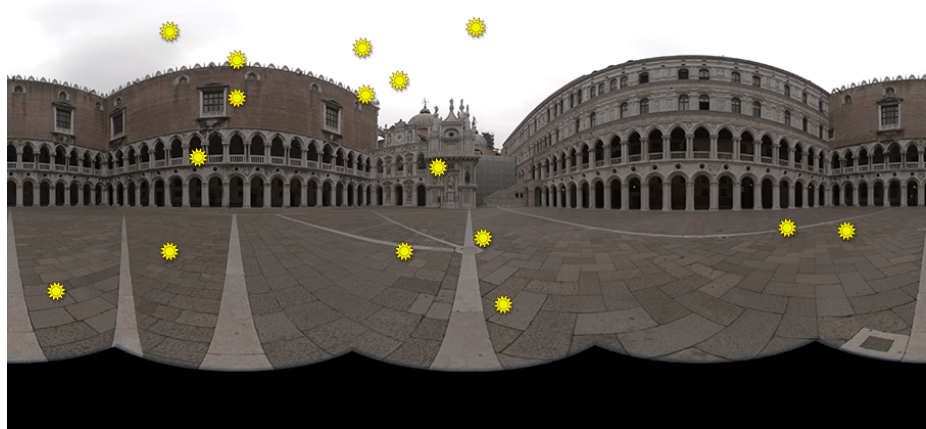


Figure 4.10: Position of calculated lights for the doge map.

CHAPTER 5

Implementation

In this chapter, we will introduce the implementation details of our method. The difference between this chapter and the previous one is that the concepts introduced in the method chapter are easily adaptable to any kind of implementation environment, while in this chapter we focus on a GPU-oriented implementation. First, we will give a general outline of our algorithm. Then, we will take each one of the single parts of the algorithm and discuss them separately. After introducing the details of the algorithm, we will discuss some caveats that are necessary in order to eliminate defects and artifacts in our algorithm. Finally, we will discuss our implementation, introducing some possible implementation alternatives in order to compare them in the result section.

5.1 Environment

In order to better contextualize some of the choices and the code parts that will be introduced in this section, we will first introduce the environment used in our implementation. The method we are going to discuss was made using the OpenGL API, version 4.3 (released in August 2012), a multi-platform API used for rendering 2D and 3D accelerated graphics. With the OpenGL API comes together GLSL, the OpenGL Shading Language, used for writing pieces

of code to be run on the GPU, called *shaders*. Our method uses some advanced features of OpenGL 4.3, so it is not immediately portable to previous generation hardware, and runs only on high-end modern GPUs. On the CPU side, we use an extended framework based on Qt, a C++ library that allows to create OpenGL contexts and graphical interfaces in an easy way.

Stuff to insert:

- Generation of random points
- Noise generation on GPU
- Sampling patterns
- Layered rendering
- Shadow mapping (for lights)
- Ping-ponging and accumulation
- Texture Views and mipmap generation (memory optimization)
- Engine structure
- Extension: compute shaders
- Extension: image load store (meh)
- Extension: cubemap
- Extension: subroutines (meh)
- Sampling colormap
- Alternative: voxelization

Caveats:

- Oversampling issues in final combinaiton (multisampling of depth map)
- Combination delta
- Shadow bias
- Random rotation

Listing 5.1: Test!

```
#version 430
layout(triangles) in;
layout(triangle_strip, max_vertices = 60) out;

#include "ss_aincludes_constants.glinc"

uniform int layers;
uniform mat4 P;
uniform mat4 viewMatrices[DIRECTIONS];

smooth in vec3 v_position[3];
smooth in vec3 v_norm[3];

smooth out vec3 position;
smooth out vec3 norm;

void main(void)
{
    int l = layers;
    for(int i = 0; i < l; i++)
    {
        gl_Layer = i;

        for(int k = 0; k < 3; k++)
        {
            vec4 v0 = gl_in[k].gl_Position;
            position = v_position[k];
            norm = v_norm[k];
            gl_Position = P * viewMatrices[i] * v0;
            EmitVertex();
        }
        EndPrimitive();
    }
}
```

In this chapter, we describe the implementation details of our technique, using the approximation of the rendering equation introduced in the previous chapter. We start by giving a rather generic introduction of our algorithm, introducing then all the implementation details.

5.2 Algorithm overview

By keeping the limitations presented in the previous chapter in mind TODO, we introduce our four pass algorithm. The algorithm is inspired by *translucent shadow maps* TODO, that we presented in chapter TODO. The general idea is to first render the scene from the light point of view, then place the disk we discussed in the method chapter TODO directly on the generated texture. We use many directions in order to capture all the sides of the object. In this section, we will assume to only have one directional light and one object in the scene. We will discuss later how to extend the method to multiple light sources.

Step 1 - Light buffer

In the first step, positions and normals of the object are rendered into a texture from the light point of view. As in standard shadow mapping we create and store a matrix to convert between world space and texture light space. With the matrix definitions and notation in section A, we express the matrix as:

$$L = T \left(\frac{1}{2} \right) \cdot S \left(\frac{1}{2} \right) \cdot P \cdot V$$

where P and V are the projection and view matrix we use to render with the light. The first two matrices are necessary to convert between clip and texture coordinates, as clip coordinates are in the range $[-1, 1] \times [-1, 1]$, while texture coordinates are in the range $[0, 1] \times [0, 1]$.

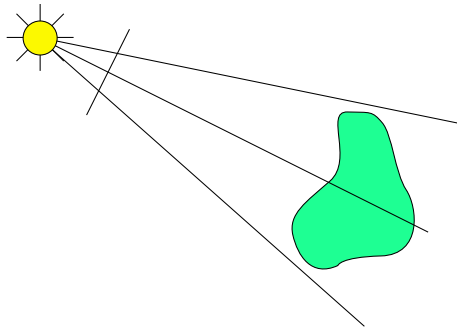


Figure 5.1: Render to G-buffer.

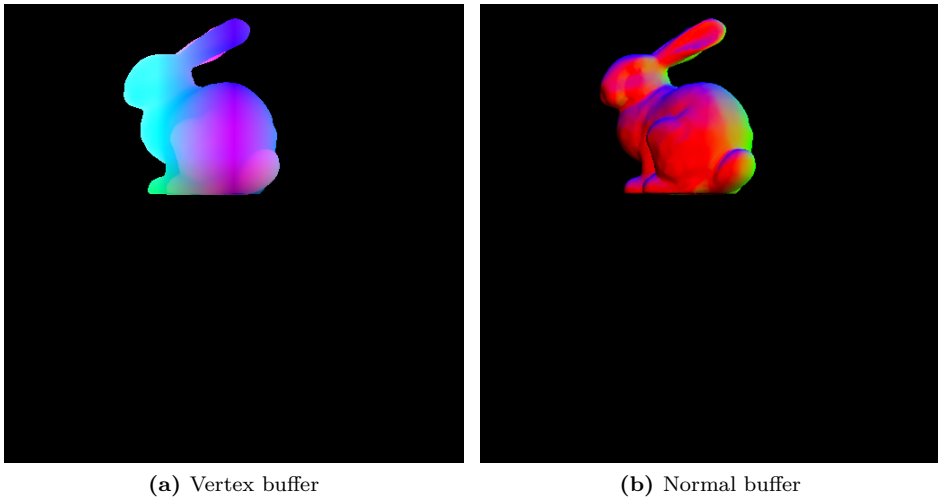


Figure 5.2: State of the vertex and normal buffer after rendering from a directional light. The model used was the Stanford bunny from the Standford 3D Scanning repository.

Step 2 - Render to array texture

In the second step, we render the object from different directions into an array texture. Each layer of the texture represents a direction from which the object is rendered to. If we are able to cover all the surface of the model, Since the BSSRDF model we are using is view-independent (apart from a Fresnel term) we can combine the results of the cubemap in a final combination step.

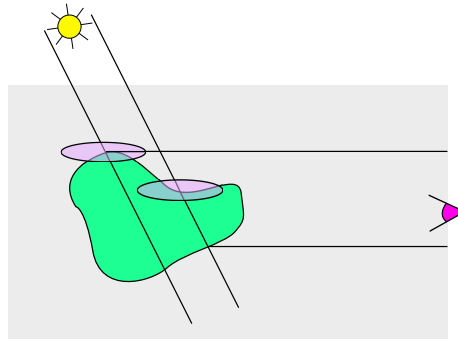


Figure 5.3: Render to cubemap.

When we are rendering a point from the orthographic camera that represents a side of the cubemap, we do as illustrated in Figure 5.4. For each fragment,

we calculate the closest point to the light, sampling the texture calculated in the previous step. In Figure 5.4 we have two examples, of when the two points coincide (directly lit) and when the two points does not (light passing through the object).

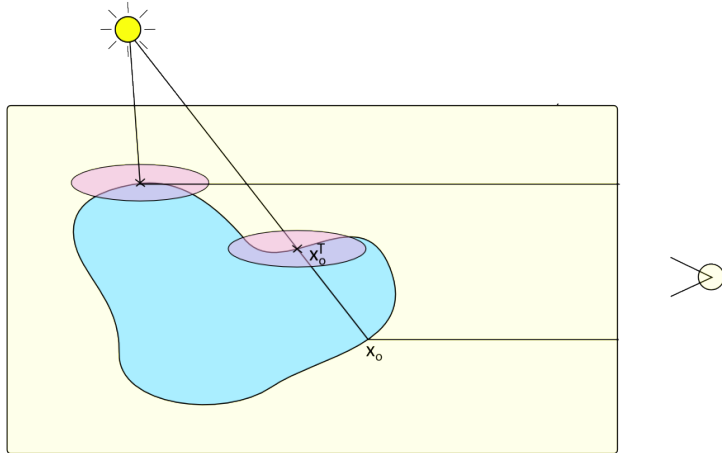


Figure 5.4: Render to cubemap, side view. Note that the fragment \mathbf{x}_o^T is not rendered in this step, but only the point \mathbf{x}_o is.

Then, we place a disk in the texture and accumulate the BSSRDF from the neighboring points, as shown in Figure 5.5. The points are chosen on the disk according to a pre-determined sampling scheme (discussed later). In order to accumulate the points and perform the right area integral, we need to assume that all the points on the disk cover the same area. So, we accumulate the point according to this formula:

$$C^f(\mathbf{x}_o) = \sum_{i=1}^k L_i(\mathbf{x}_i, \vec{\omega}_i) S_i(\mathbf{x}_i, \mathbf{x}_o, \vec{\omega}_i, \vec{\omega}_o) (\vec{n}_i \cdot \vec{\omega}_i) F_t(\vec{n}_i, \vec{\omega}_i)$$

where \mathbf{x}_o is the exiting point C^f is the cubemap on face f , L_i is the incoming radiance, S_i is the BSSRDF, \mathbf{x}_i and \vec{n}_i are the position and the normal sampled from a point of the disc, k is the number of samples, and F_t is the incoming Fresnel term.

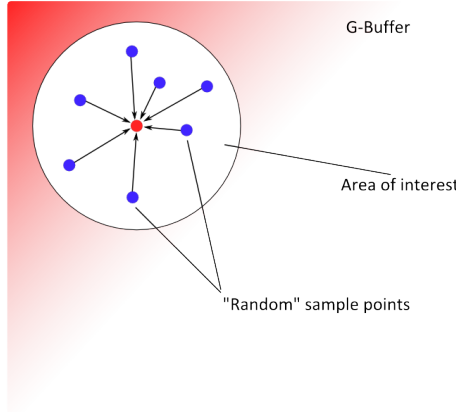


Figure 5.5: Render to cubemap, gbuffer view.

Step 3 - Combination

In this step, for each fragment on the surface we sample all the six cubemap sides as illustrated in Figure 5.6. In order to do this, we need a depth cubemap that inform us if the fragment was visible when we rendered the cubemap face. Then, each point is divided by the number of visible faces to average it. In formulas, to get the final luminance:

$$L(\mathbf{x}) = \frac{\sum_{i=1}^6 V_i C(\mathbf{x}_{proj}^i)}{\sum_{i=1}^6 V_i}$$

where V_i is a visibility function that is zero if the point is not visible on the face i and 1 if it is visible. $C(\mathbf{x})$ is the sample from the cubemap obtained in the previous step, and \mathbf{x}_{proj}^i is the point \mathbf{x} projected on the i -th cubemap face.

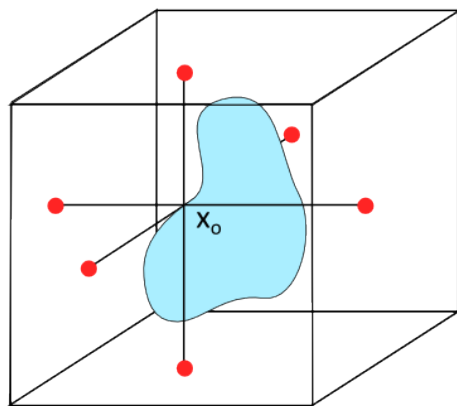


Figure 5.6: Final combination step. Note that the point is generally not visible from all the cubemap faces.

5.3 Implementation details

5.4 Artifacts

A simple implementation of the method described until now is not completely correct. In fact, since we are discretizing the surface on a texture, some sampling artifacts are inevitable. During our implementation we identified three different types of artifacts:

- Incorrect sampling of the G-buffer
- Incorrect sampling of the cubemap
- Shadow bias (when sampling the depth of the texture).

That are described in detail in the following sections.

5.4.1 Incorrect sampling of the G-buffer

In order to sample the G-buffer correctly, we need to modify the world coordinate of the point \mathbf{x}_o with normal \vec{n}_o in order to "shrink" a little bit towards the inside of the object according to the light direction $\vec{\omega}_l$:

$$\mathbf{x}'_o = \mathbf{x}_o - \epsilon_g (\vec{n}_o - \vec{\omega}_l (\vec{\omega}_l \cdot \vec{n}_o))$$

5.4.2 Incorrect sampling of the cubemap

Since we are sampling a cubemap, we do not need to account for the light direction in this case. In addition, the cubemap needs a 3D vector to be sampled with. So, instead of using \mathbf{x}_o , we use a point slightly intruded (i.e. displaced along the normal) in the calculations, according to:

$$\mathbf{x}'_o = \mathbf{x}_o - \epsilon_c \vec{n}_o$$

5.4.3 Shadow bias

In order to avoid artifacts such as shadows acne, we use a bias when comparing the z values of a point to determine if the point is in shadow or not. This implies that we need to convert the depth value from texture space (\mathbf{z}_{tex}) to world space again (\mathbf{z}_{world}). Since we are using an orthographics camera, the z value is the same in clip coordinates and in normalized device coordinates. Then, we simply use the camera projection properties (\mathbf{z}_{far} , \mathbf{z}_{near}) to convert the depth into the camera local space, in order to finally add the camera position transformed z value (\mathbf{z}_{camera}) and reconstruct the depth in world space:

$$\mathbf{z}_{world} = \mathbf{z}_{camera} - \frac{\mathbf{z}_{far} - \mathbf{z}_{near}}{2} \left(2\mathbf{z}_{tex} - 1 + \frac{\mathbf{z}_{far} + \mathbf{z}_{near}}{\mathbf{z}_{far} - \mathbf{z}_{near}} \right)$$

And finally compare the obtained z with the z position in world space of the point (\mathbf{z}) using the bias ϵ_b , so a point is lit iff:

$$\mathbf{z}_{world} - \epsilon_b < \mathbf{z}$$

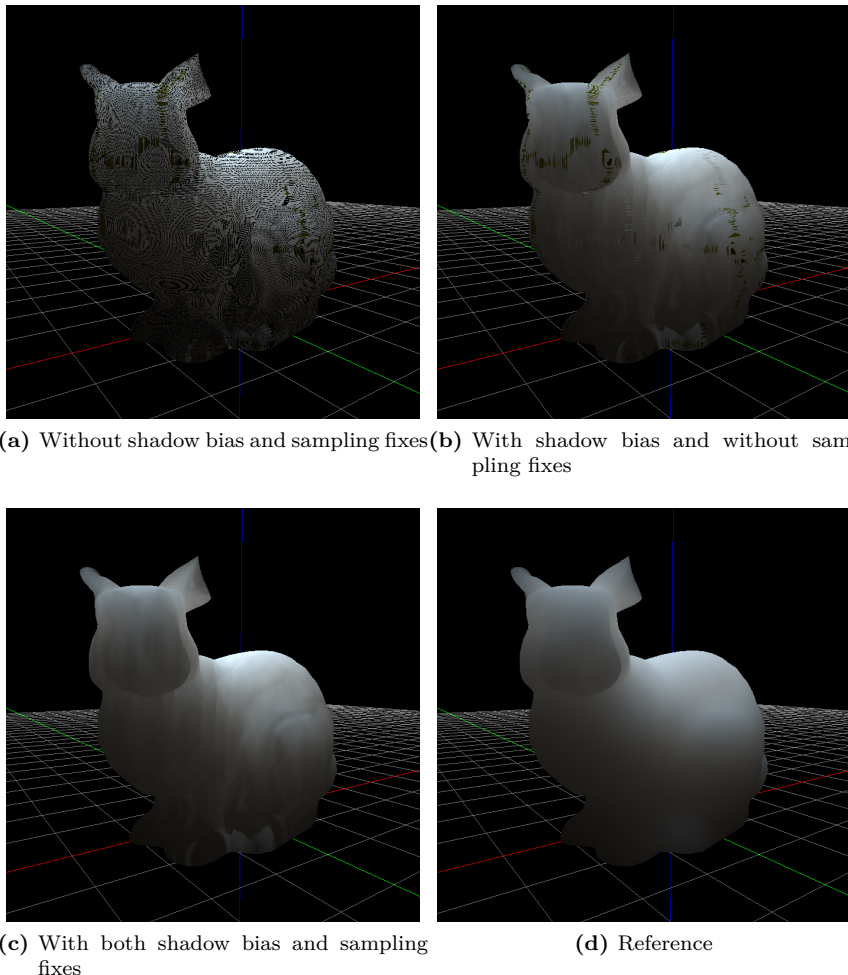


Figure 5.7: Progressively removing artifacts to get to the final image.

CHAPTER 6

Results

APPENDIX A

Model matrices

A.1 Model matrices

Translation matrix

$$T(\mathbf{t}) = \begin{bmatrix} 1 & 0 & 0 & \mathbf{t}_x \\ 0 & 1 & 0 & \mathbf{t}_y \\ 0 & 0 & 1 & \mathbf{t}_z \\ 0 & 0 & 0 & 1 \end{bmatrix}$$

Rotation matrix

$$R_x(\theta) = \begin{bmatrix} 1 & 0 & 0 & 0 \\ 0 & \cos \theta & -\sin \theta & 0 \\ 0 & \sin \theta & \cos \theta & 0 \\ 0 & 0 & 0 & 1 \end{bmatrix}$$

$$R_y(\theta) = \begin{bmatrix} \cos \theta & 0 & \sin \theta & 0 \\ 0 & 1 & 0 & 0 \\ -\sin \theta & 0 & \cos \theta & 0 \\ 0 & 0 & 0 & 1 \end{bmatrix}$$

$$R_z(\theta) = \begin{bmatrix} \cos \theta & -\sin \theta & 0 & 0 \\ \sin \theta & \cos \theta & 0 & 0 \\ 0 & 0 & 1 & 0 \\ 0 & 0 & 0 & 1 \end{bmatrix}$$

Scale matrix

$$S(s) = \begin{bmatrix} s_x & 0 & 0 & 0 \\ 0 & s_y & 0 & 0 \\ 0 & 0 & s_z & 0 \\ 0 & 0 & 0 & 1 \end{bmatrix}$$

A.2 View Matrix

e is the camera position, **d** is the camera direction, **u** is the up vector.

$$\begin{aligned}\vec{c} &= -\frac{\mathbf{d}}{\|\mathbf{d}\|} \\ \vec{a} &= \frac{\vec{c} \times \mathbf{u}}{\|\vec{c} \times \mathbf{u}\|} \\ \vec{b} &= \vec{a} \times \vec{c}\end{aligned}$$

$$V(\mathbf{e}, \mathbf{d}, \mathbf{u}) = \begin{bmatrix} \vec{a}_x & \vec{a}_y & \vec{a}_z & -\mathbf{e}_x \\ \vec{b}_x & \vec{b}_y & \vec{b}_z & -\mathbf{e}_y \\ \vec{c}_x & \vec{c}_y & \vec{c}_z & -\mathbf{e}_z \\ 0 & 0 & 0 & 1 \end{bmatrix}$$

A.3 Projection Matrix

Orthographic matrix

\mathbf{l} is the left bottom near corner of the frustum, \mathbf{r} is the top right far corner.

$$O(\mathbf{l}, \mathbf{r}) = \begin{bmatrix} \frac{2}{\mathbf{r}_x - \mathbf{l}_x} & 0 & 0 & -\frac{\mathbf{r}_x + \mathbf{l}_x}{\mathbf{r}_x - \mathbf{l}_x} \\ 0 & \frac{2}{\mathbf{r}_y - \mathbf{l}_y} & 0 & -\frac{\mathbf{r}_y + \mathbf{l}_y}{\mathbf{r}_y - \mathbf{l}_y} \\ 0 & 0 & -\frac{2}{\mathbf{r}_z - \mathbf{l}_z} & -\frac{\mathbf{r}_z + \mathbf{l}_z}{\mathbf{r}_z - \mathbf{l}_z} \\ 0 & 0 & 0 & 1 \end{bmatrix}$$

Perspective matrix

fov is the field of view in radians, A is the aspect ratio, n_p is the near camera plane and f_p is the far camera plane. We define:

$$f_c = \frac{1}{\tan(\frac{fov}{2})}$$

$$P(fov, A, n, f) = \begin{bmatrix} \frac{f_c}{A} & 0 & 0 & 0 \\ 0 & f_c & 0 & 0 \\ 0 & 0 & \frac{n+f}{n-f} & \frac{2nf}{n-f} \\ 0 & 0 & -1 & 0 \end{bmatrix}$$

Bibliography

- Michael Ashikmin, Simon Premože, and Peter Shirley. A microfacet-based brdf generator. In *Proceedings of the 27th Annual Conference on Computer Graphics and Interactive Techniques*, SIGGRAPH '00, pages 65–74, New York, NY, USA, 2000. ACM Press/Addison-Wesley Publishing Co. URL <http://dx.doi.org/10.1145/344779.344814>.
- Jesper Børslum, Brian Bunch Christensen, Thomas Kim Kjeldsen, Peter Trier Mikkelsen, Karsten Østergaard Noe, Jens Rimestad, and Jesper Mosegaard. Sslpv: Subsurface light propagation volumes. In *Proceedings of the ACM SIGGRAPH Symposium on High Performance Graphics*, HPG '11, pages 7–14, New York, NY, USA, 2011. ACM. URL <http://doi.acm.org/10.1145/2018323.2018325>.
- Michael F. Cohen, John Wallace, and Pat Hanrahan. *Radiosity and Realistic Image Synthesis*. Academic Press Professional, Inc., San Diego, CA, USA, 1993.
- Carsten Dachsbacher and Marc Stamminger. Translucent shadow maps. In *Proceedings of the 14th Eurographics Workshop on Rendering*, EGRW '03, pages 197–201, Aire-la-Ville, Switzerland, Switzerland, 2003. Eurographics Association. URL <http://dl.acm.org/citation.cfm?id=882404.882433>.
- B. Davison and John Bradbury Sykes. *Neutron transport theory*. Oxford University Press, 1958.
- Eugene D'Eon. A better dipole (a publicly available manuscript). Technical report, -, 2012. URL <http://www.eugenedeon.com/papers/betterdipole.pdf>.

Eugene D'Eon and Geoffrey Irving. A quantized-diffusion model for rendering translucent materials. In *ACM SIGGRAPH 2011 Papers*, SIGGRAPH '11, pages 56:1–56:14, New York, NY, USA, 2011. ACM. URL <http://doi.acm.org/10.1145/1964921.1964951>.

Eugene d'Eon, David Luebke, and Eric Enderton. Efficient rendering of human skin. In *Proceedings of the 18th Eurographics Conference on Rendering Techniques*, EGSR'07, pages 147–157, Aire-la-Ville, Switzerland, Switzerland, 2007. Eurographics Association. URL <http://dx.doi.org/10.2312/EGWR/EGSR07/147-157>.

Agns Desolneux, Lionel Moisan, and Jean-Michel Morel. *From Gestalt Theory to Image Analysis: A Probabilistic Approach*. Springer Publishing Company, Incorporated, 1st edition, 2007.

Craig Donner and Henrik Wann Jensen. Light diffusion in multi-layered translucent materials. In *ACM SIGGRAPH 2005 Papers*, SIGGRAPH '05, pages 1032–1039, New York, NY, USA, 2005. ACM. URL <http://doi.acm.org/10.1145/1186822.1073308>.

Craig Donner, Jason Lawrence, Ravi Ramamoorthi, Toshiya Hachisuka, Henrik Wann Jensen, and Shree Nayar. An empirical bssrdf model. *ACM Trans. Graph.*, 28(3):30:1–30:10, July 2009. URL <http://doi.acm.org/10.1145/1531326.1531336>.

Craig Steven Donner. *Towards Realistic Image Synthesis of Scattering Materials*. PhD thesis, University of California, San Diego, La Jolla, CA, USA, 2006. AAI3226771.

Julie Dorsey, Alan Edelman, Henrik Wann Jensen, Justin Legakis, and Hans Køhling Pedersen. Modeling and rendering of weathered stone. In *Proceedings of the 26th Annual Conference on Computer Graphics and Interactive Techniques*, SIGGRAPH '99, pages 225–234, New York, NY, USA, 1999. ACM Press/Addison-Wesley Publishing Co. URL <http://dx.doi.org/10.1145/311535.311560>.

Raanan Fattal. Participating media illumination using light propagation maps. *ACM Trans. Graph.*, 28(1):7:1–7:11, February 2009. URL <http://doi.acm.org/10.1145/1477926.1477933>.

J. R. Frisvad, T. Hachisuka, and T. K. Kjeldsen. Directional dipole for subsurface scattering in translucent materials. Technical report, DTU Compute, 2013. URL <http://www2.imm.dtu.dk/pubdb/p.php?6646>. Unpublished manuscript.

Robin Green. Spherical harmonic lighting: The gritty details, January 2003. Sony Computer Entertainment America.

- Akira Ishimaru. *Wave propagation and scattering in random media*. IEEE, 1997.
- ITU. Parameter values for the hdtv standards for production and international programme exchange. Technical Report ITU-R BT.709-2, ITU-R, June 2001. URL <http://www.itu.int/rec/R-REC-BT.709-2-199510-S/en>.
- Henrik Wann Jensen and Juan Buhler. A rapid hierarchical rendering technique for translucent materials. *ACM Trans. Graph.*, 21(3):576–581, July 2002. URL <http://doi.acm.org/10.1145/566654.566619>.
- Henrik Wann Jensen and Per H. Christensen. Efficient simulation of light transport in scenes with participating media using photon maps. In *Proceedings of the 25th Annual Conference on Computer Graphics and Interactive Techniques*, SIGGRAPH ’98, pages 311–320, New York, NY, USA, 1998. ACM. URL <http://doi.acm.org/10.1145/280814.280925>.
- Henrik Wann Jensen, Stephen R. Marschner, Marc Levoy, and Pat Hanrahan. A practical model for subsurface light transport. In *Proceedings of the 28th Annual Conference on Computer Graphics and Interactive Techniques*, SIGGRAPH ’01, pages 511–518, New York, NY, USA, 2001. ACM. URL <http://doi.acm.org/10.1145/383259.383319>.
- Jorge Jimenez, Veronica Sundstedt, and Diego Gutierrez. Screen-space perceptual rendering of human skin. *ACM Trans. Appl. Percept.*, 6(4):23:1–23:15, October 2009. URL <http://doi.acm.org/10.1145/1609967.1609970>.
- J. H. Joseph, W. J. Wiscombe, and J. A. Weinman. The delta-Eddington approximation for radiative flux transfer. *Journal of Atmospheric Sciences*, 33:2452–2459, December 1976.
- Anton Kaplanyan and Carsten Dachsbacher. Cascaded light propagation volumes for real-time indirect illumination. In *Proceedings of the 2010 ACM SIGGRAPH Symposium on Interactive 3D Graphics and Games*, I3D ’10, pages 99–107, New York, NY, USA, 2010. ACM. URL <http://doi.acm.org/10.1145/1730804.1730821>.
- Hendrik P. A. Lensch, Michael Goesele, Philippe Bekaert, Jan Kautz, Marcus A. Magnor, Jochen Lang, and Hans-Peter Seidel. Interactive rendering of translucent objects. In *Proceedings of the 10th Pacific Conference on Computer Graphics and Applications*, PG ’02, pages 214–, Washington, DC, USA, 2002. IEEE Computer Society. URL <http://dl.acm.org/citation.cfm?id=826030.826632>.
- Tom Mertens, J. Kautz, P. Bekaert, F. Van Reeth, and H.-P. Seidel. Efficient rendering of local subsurface scattering. In *Computer Graphics and Applications, 2003. Proceedings. 11th Pacific Conference on*, pages 51–58, Oct 2003a.

- Tom Mertens, Jan Kautz, Philippe Bekaert, Hans-Peter Seidelz, and Frank Van Reeth. Interactive rendering of translucent deformable objects. In *Proceedings of the 14th Eurographics Workshop on Rendering*, EGRW '03, pages 130–140, Aire-la-Ville, Switzerland, Switzerland, 2003b. Eurographics Association. URL <http://dl.acm.org/citation.cfm?id=882404.882423>.
- Rosana Montes and Carlos Ureña. An overview of brdf models. -, -:, 2012.
- Srinivasa G. Narasimhan, Mohit Gupta, Craig Donner, Ravi Ramamoorthi, Shree K. Nayar, and Henrik Wann Jensen. Acquiring scattering properties of participating media by dilution. *ACM Trans. Graph.*, 25(3):1003–1012, July 2006. URL <http://doi.acm.org/10.1145/1141911.1141986>.
- Matt Pharr and Pat Hanrahan. Monte carlo evaluation of non-linear scattering equations for subsurface reflection. In *Proceedings of the 27th Annual Conference on Computer Graphics and Interactive Techniques*, SIGGRAPH '00, pages 75–84, New York, NY, USA, 2000. ACM Press/Addison-Wesley Publishing Co. URL <http://dx.doi.org/10.1145/344779.344824>.
- Matt Pharr and Greg Humphreys. *Physically Based Rendering: From Theory to Implementation*. Morgan Kaufmann Publishers Inc., San Francisco, CA, USA, 2004.
- M.A. Shah, J. Konttinen, and S. Pattanaik. Image-space subsurface scattering for interactive rendering of deformable translucent objects. *Computer Graphics and Applications, IEEE*, 29(1):66–78, Jan 2009.
- Peter-Pike Sloan. Stupid spherical harmonics (sh) tricks. In *Game Developers Conference 2008, February 2008 (updated 2/10/2010)*, 2008.
- Jos Stam. Multiple scattering as a diffusion process. In PatrickM. Hanrahan and Werner Purgathofer, editors, *Rendering Techniques 1995*, Eurographics, pages 41–50. Springer Vienna, 1995. URL http://dx.doi.org/10.1007/978-3-7091-9430-0_5.
- Anna Tomaszewska and Krzysztof Stefanowski. Real-time spherical harmonics based subsurface scattering. In Aurélio Campilho and Mohamed Kamel, editors, *Image Analysis and Recognition*, volume 7324 of *Lecture Notes in Computer Science*, pages 402–409. Springer Berlin Heidelberg, 2012. URL http://dx.doi.org/10.1007/978-3-642-31295-3_47.
- Unity. *Unity Manual: Forward Rendering Path Details*, 2012. URL <http://docs.unity3d.com/Manual/RenderTech-ForwardRendering.html>.
- Yajun Wang, Jiaping Wang, Nicolas Holzschuch, Kartic Subr, Jun-Hai Yong, and Baining Guo. Real-time rendering of heterogeneous translucent objects with arbitrary shapes. *Comput. Graph. Forum*, 29(2):497–506, 2010. URL <http://dblp.uni-trier.de/db/journals/cgf/cgf29.html#WangWHSYG10>.